Aberrations in Notch-Hedgehog signalling reveal cancer stem cells harbouring conserved oncogenic properties associated with hypoxia and immunoevasion

Running title: Pan-cancer signature of Notch-Hedgehog signalling

Wai Hoong Chang[1] and Alvina G. Lai[1]

[1]Institute of Health Informatics, University College London,

222 Euston Road, London NW1 2DA, United Kingdom

For correspondence: Alvina.Lai@ucl.ac.uk; alvinagracelai@gmail.com

Phone: +44 20 3549 5771

18 Abstract

19 Background:

20 Cancer stem cells (CSCs) have innate abilities to resist even the harshest of therapies. To
21 eradicate CSCs, parallels can be drawn from signalling modules that orchestrate pluripotency.
22 Notch-Hedgehog hyperactivation are seen in CSCs, yet, not much is known about their
23 conserved roles in tumour progression across cancers.

24 Methods:

25 Employing a comparative approach involving 21 cancers, we uncovered clinically-relevant,
26 pan-cancer drivers of Notch and Hedgehog. GISTIC datasets were used to evaluate copy
27 number alterations. Receiver operating characteristic and Cox regression were employed for
28 survival analyses.

29 Results:

30 We identified a Notch-Hedgehog signature of 13 genes exhibiting high frequencies of somatic
31 amplifications leading to transcript overexpression. The signature successfully predicted
32 patients at risk of death in five cancers(n=2,278): glioma(P<0.0001), clear cell renal
33 cell(P=0.0022), papillary renal cell(P=0.00099), liver(P=0.014) and stomach(P=0.011). The
34 signature was independent of other clinicopathological parameters and offered additional
35 resolution to stratify similarly-staged tumours. High-risk patients exhibited features of
36 stemness and had more hypoxic tumours, suggesting that hypoxia may influence CSC
37 behaviour. Notch-Hedgehog^{+} CSCs had an immune privileged phenotype associated with
38 increased regulatory T cell function.

39 Conclusion: This study will set the stage for exploring adjuvant therapy targeting the Notch-
40 Hedgehog axis to help optimise therapeutic regimes leading to successful CSC elimination.

41 Background:

42 Tumours are far from homogeneous masses, yet many contemporary therapies continue to
43 treat them as such. It has become increasingly clear that a minor population of tumour cells
44 known as cancer stem cells (CSCs) contribute to treatment resistance as they have the
45 propensity to tolerate DNA damage(1,2) and evade immune detection(3) to give rise to new
46 tumours post therapy. Identification of CSCs has remained a challenging endeavour since
47 they only make up a small proportion of the tumour and are histologically similar to non-
48 stem cancer cells. Moreover, molecular markers that identify CSCs are often cancer-type
49 dependent, which limit their broad scale applications(4). CSCs share many qualities with
50 embryonic or adult stem cells. For example, activation of signalling pathways involved in
51 coordinating cellular homeostasis, morphogenesis and cell fate determination (TGF-β, Wnt,
52 Notch and Hedgehog) are often seen in CSCs. These pathways rarely act in isolation and
53 significant crosstalk between them have been reported(5).

54

55 In order to fully exploit these pathways for CSC therapy, pan-cancer explorations are
56 warranted to reveal conserved components that can be prioritised as therapeutic targets.
57 Concentrating on Notch and Hedgehog signalling pathways, we seek to attain a
58 comprehensive understanding of how somatic copy number alterations and expression
59 profiles of pathway genes along with their downstream targets could influence tumour
60 progression and prognosis. The role of Notch signalling in oncogenesis was initially
61 discovered in T cell acute lymphoblastic leukaemia(6). Since then, multiple studies on Notch
62 signalling have demonstrated both oncogenic and tumour suppressive functions in
63 haematological and solid malignancies, implying its pleiotropic nature that is very much
64 dependent on cellular types(7). Hedgehog is a morphogen that regulates a signalling cascade

65 involving the Smoothened protein to influence morphogenetic processes such as
66 proliferation and differentiation(8). Interactions between Notch and Hedgehog signalling
67 have been demonstrated in multiple cancers. *Hes1*, a Notch effector, is targeted by *sonic*
68 *hedgehog* in neural cells(9). When *Patched*, a negative regulator of Hedgehog, is abrogated in
69 mice, this gives rise to medulloblastoma with enhanced Notch signalling(10). Hedgehog
70 signalling promotes the expression of *Jagged2* (a Notch ligand)(11) and in ovarian cancer
71 mice models, inhibition of *Jagged1* would sensitise tumours to docetaxel treatment by
72 affecting *GLI2* function(12). Concurrent activation of Hedgehog and Notch signalling was
73 observed in prostate cancer cells that were resistant to docetaxel(13). Glioblastoma treated
74 with a Notch inhibitor was subsequently desensitised to further Notch suppression as they
75 upregulate Hedgehog signalling(14).
76
77 These studies highlight the importance of Notch-Hedgehog interactions in cancer, which calls
78 for a better understanding of their relationship and also to reveal crosstalk with other
79 pathways involved in regulating CSC function. Harnessing genomic and transcriptomic
80 sequences of 21 cancer types, we performed a comprehensive investigation linking genomic
81 alterations to transcriptional dysregulation of Notch-Hedgehog pathway genes. We
82 discovered conserved patterns of Notch-Hedgehog hyperactivation across cancers and
83 revealed putative driver genes that were associated with CSC phenotypes underpinning poor
84 clinical outcomes. We also examined the relationship between the tumour
85 microenvironment (hypoxia and immune suppression) and Notch-Hedgehog^{+} CSCs. In-depth
86 knowledge of the Notch-Hedgehog signalling axis afforded by this study will set the stage for
87 exploring combinatorial chemotherapy targeting both pathways simultaneously to potentially
88 eradicate CSCs.

89 Materials and Methods:

90 A total of 72 genes associated with Notch and Hedgehog signalling were retrieved from the
91 Kyoto Encyclopedia of Genes and Genomes (KEGG) database listed in Table S1.

92

93 Study cohorts

94 We retrieved transcriptomic and genomic profiles of 21 cancer types (n=18,484) including
95 their non-tumour counterparts from The Cancer Genome Atlas and Broad Institute GDAC
96 Firehose(15) (Table S2).

97

98 Somatic copy number alterations analyses

99 We retrieved Firehose Level 4 copy number variation datasets in the form of GISTIC gene-
100 level tables, which provided discrete amplification and deletion indicators(16). A sample was
101 defined as 'deep amplification' for values that were higher than the maximum median copy-
102 ratio for each chromosome arm (+2). Samples with values less than the minimum median
103 copy-ratio for each chromosome arm were called 'deep deletions' (-2). GISTIC indicators of
104 +1 and -1 represented shallow amplifications and deletions respectively.

105

106 Calculating Notch-Hedgehog 13-gene scores, hypoxia scores and regulatory T cell (Treg) scores

107 The Notch-Hedgehog 13-gene signature was employed to calculate a score for each patient.
108 It comprised of the following genes: *JAG1, LFNG, DTX2, DLL3, GPR161, PSENEN, GLI1, HES1,*
109 *PTCRA, DTX3L, ADAM17, KIF7* and *NOTCH1*. Hypoxia scores were calculated from 52 hypoxia
110 signature genes(17). Treg scores were calculated based on the overlap between four Treg
111 signatures(18–21), consisting of 31 genes: *FOXP3, TNFRSF18, TNFRSF9, TIGIT, IKZF2, CTLA4,*
112 *CCR8, TNFRSF4, IL2RA, BATF, IL2RB, CTSC, CD27, PTTG1, ICOS, CD7, TFRC, ERI1, GLRX, NCF4,*

113 *PARK7, HTATIP2, FCRL3, CALM3, DPYSL2, CSF2RB, CSF1, IL1R2, VDR, ACP5* and *MAGEH1*.
114 Scores were calculated from the average $\log_2$ expression values of 13, 52 or 31 genes
115 representing Notch-Hedgehog, hypoxia and Tregs respectively. Kaplan-Meier analyses of the
116 Notch-Hedgehog signature were performed on patients separated into quartiles based on
117 their 13-gene scores. For analyses in Figures 4, 5 and 6, patients were separated into four
118 groups using median 13-gene scores and median CSC transcription factor expression levels
119 (*EZH2, REST* and *SUZ12*), hypoxia scores or Treg scores as thresholds for Kaplan-Meier and
120 Cox regression analyses. Nonparametric Spearman's rank-order correlation tests were used
121 to investigate the relationship between 13-gene scores and TF expression levels, hypoxia
122 scores or Treg scores.
123
124 Multidimensional scaling, differential expression and survival analyses
125 As per the journal's guidelines, we have not repeated methods here as we have previously
126 published detail methods for multidimensional scaling (MDS), differential expression and
127 survival analyses(22–24). Briefly, MDS analysis was employed to visualise samples' distance
128 (tumour and non-tumour) in reduced 2-dimensional space. The R vegan package was
129 employed for MDS ordination using Euclidean distances. Permutational multivariate analysis
130 of variance (PERMANOVA) was used to investigate statistical differences between tumour
131 and non-tumour samples. The linear model and Bayes method was employed for differential
132 expression analyses, followed by the Benjamini-Hochberg false discovery rate method.
133 Kaplan-Meier, Cox proportional hazards and receiver operating characteristic survival
134 analyses were performed using R survminer, survival and survcomp packages.
135
136 Functional enrichment and transcription factor (TF) analyses

137 Differential expression analyses as mentioned previously were performed on patients
138 separated into quartiles 4 and 1 based on their 13-gene scores. Differentially expressed
139 genes were mapped against KEGG and Gene Ontology (GO) databases using GeneCodis(25)
140 to determine pathways that were enriched. The Enrichr tool was used to determine whether
141 differentially expressed genes were enriched for stem cell TFs binding targets by comparing
142 chromatin immunoprecipitation sequencing profiles from ChEA and ENCODE databases(26).
143
144 The R ggplot2 and pheatmap packages were used to generate all plots.

145 Results:

146

147 **Recurrently amplified driver genes associated with Notch and Hedgehog activation in 21**

148 **diverse cancer types**

149

150 To characterise the extent of Notch and Hedgehog signalling and identify common molecular

151 subtypes, we examined somatic copy number alterations (SCNAs) and differential expression

152 (tumour versus non-tumour) patterns of 72 genes in 18,484 cases of clinically annotated

153 stage I to IV samples representing 21 cancer types (Fig. 1A; Table S1; Table S2). We found

154 that 70 out of 72 genes were recurrently amplified in at least 20% of samples per cancer type

155 in at least one cancer type (Fig. 1A). Lung squamous cell carcinoma (LUSC) had the highest

156 fraction of samples harbouring amplified Hedgehog genes, while endometrial cancer (UCEC)

157 had the fewest somatic gains (Fig. 1B). When considering Notch gene amplifications, LUSC

158 also emerged as the top candidate while clear cell renal cell carcinoma (KIRC) had the fewest

159 number of Notch gene amplifications (Fig. 1B). In terms of focal deletions, this was also the

160 highest in LUSC for Hedgehog genes and renal chromophobe carcinoma (KICH) for Notch

161 genes (Fig. 1B).

162

163 Focusing on recurrently amplified genes, we identified 35 genes (Hedgehog pathway: 13

164 genes; Notch pathway: 22 genes) that were gained in >20% of samples and in at least one-

165 third of cancer types (> 7 cancers) (Fig. 1C). *GLI3, SMURF1, RBPJL, JAG1, LFNG* and *DTX2* were

166 some of the most amplified genes present in at least 18 cancers (Fig. 1C). In contrast, *KIF7,*

167 *NOTCH1, MAML* and *ADAM17* were the least amplified genes (Fig. 1C). LUSC had the highest

168 number of amplified genes (34 genes) followed by 33 genes in oesophageal carcinoma (ESCA)

169 and stomach and oesophageal carcinoma (STES) and 32 genes in stomach adenocarcinoma
170 (STAD) and bladder urothelial carcinoma (BLCA) (Fig. 1C). In contrast, only 8 genes were
171 amplified in UCEC (Fig. 1C).
172
173 SCNA events associated with overexpression could represent candidate driver genes since
174 positive correlations between gene amplification and overexpression are indicative of a gain-
175 of-function(27). Differential expression analyses between tumour and adjacent non-tumour
176 samples revealed that 13 of the amplified genes were also significantly upregulated (> 1.5
177 fold-change, P<0.05) in tumours of at least 7 cancer types (Fig. 1C). These genes were
178 prioritised as a Notch-Hedgehog signature potentially representative of multiple cancers:
179 *JAG1, LFNG, DTX2, DLL3, GPR161, PSENEN, GLI1, HES1, PTCRA, DTX3L, ADAM17, KIF7* and
180 *NOTCH1* (Fig. 1C).
181
182
183 A 13-gene Notch-Hedgehog signature predicts survival outcomes in five cancers
184
185 Tumours displayed various degrees of somatic gains and overexpression of Notch-Hedgehog
186 pathway genes (Fig. 1), suggesting that aberrant activation of these pathways may influence
187 disease progression and survival outcomes. We employed univariate Cox proportional
188 hazards regression analyses to test the prognostic roles of individual Notch-Hedgehog
189 signature genes across 20 cancer types where survival data is available. Prognosis appeared
190 to tissue type-dependent (Fig. S1). All 13 genes were prognostic in the glioma dataset
191 (GBMLGG), consisting of samples from patients with astrocytoma, oligoastrocytoma,
192 oligodendroglioma and glioblastoma multiforme (Fig. S1). A majority of the genes (9 out of

193 13) were associated with poor prognosis (hazard ratio [HR] > 1, P<0.05) (Fig. S1). However,
194 despite showing high frequencies of SCNAs (Fig. 1C), none of the 13 genes harboured
195 prognostic information in patients with LUSC, cholangiocarcinoma (CHOL) or oesophageal
196 carcinoma (ESCA) (Fig. S1).
197
198 We next considered all 13 genes as a group in assessing prognosis. For each patient, we
199 calculated their 13-gene scores by taking the average expression of all genes. Patients were
200 separated into survival quartiles based on their 13-gene scores. Remarkably, Kaplan-Meier
201 estimates and log-rank tests revealed that the 13-gene signature accurately predicted
202 patients at higher risk of death in five cancer types (n=2,278): glioma (P<0.0001), clear cell
203 renal cell (P=0.0022), papillary renal cell (P=0.00099), liver (P=0.014) and stomach (P=0.011)
204 (Fig. 2A). Patients within the 4th quartile had significantly poorer survival rates compared to
205 those within the 1st quartile: glioma (HR=3.386, P<0.0001), clear cell renal cell (HR=2.177,
206 P=0.00048), papillary renal cell (HR=4.881, P=0.0053), liver (HR=2.627, P=0.0039) and
207 stomach (HR=2.217, P=0.014) (Table S3). When comparing tumour and non-tumour
208 expression patterns, Mann-Whitney-Wilcoxon tests revealed that a vast majority of the 13
209 genes were significantly upregulated in tumours of these cancers (Fig. S2) where
210 hyperactivation of Notch-Hedgehog signalling was associated with adverse survival outcomes
211 (Fig. 2A). Multidimensional scaling analyses revealed that the 13 genes could accurately
212 distinguish tumour from non-tumour samples in these cancers (Fig. 2B), suggesting that
213 Notch-Hedgehog transcriptional states could be used to identify cells with oncogenic
214 properties.
215

216 Multivariate Cox proportional hazards regression was used to determine whether the
217 signature was confounded by other clinicopathological features. Tumour, node, metastasis
218 (TNM) staging is frequently used for patient stratification. Even after accounting for TNM
219 staging, the signature remained an independent predictor of survival: clear cell renal cell
220 (HR=1.731, P=0.014), papillary renal cell (HR=2.297, P=0.042), liver (HR=2.146; P=0.024) and
221 stomach (HR=2.161, P=0.017) (Table S3). Given that both the signature and tumour stage
222 were independent of each other, we reason that the signature could be used to improve
223 TNM staging. We observed that Notch-Hedgehog driver genes offered an additional
224 resolution in tumour classification for further stratification of similarly staged tumours in
225 these cancers: clear cell renal cell (P<0.0001), papillary renal cell (P<0.0001), liver (P<0.0001)
226 and stomach (P=0.0068) (Fig. 3A).
227
228 Glioma samples are classified into four histological categories with varying severity: low-
229 grade astrocytoma, low-grade oligodendroglioma, low-grade oligoastrocytoma (consisting of
230 both abnormal astrocytoma and oligodendroglioma cells), and grade IV glioblastoma
231 multiforme. Kaplan-Meier analyses of glioma samples grouped by histology revealed that the
232 signature remained prognostic in astrocytoma (P=0.038), oligoastrocytoma (P=0.0018) and
233 glioblastoma multiforme (P=0.045) (Fig. 3B). Patients with low-grade gliomas stratified by the
234 signature into the 4th quartile had significantly higher death risks compared to those within
235 the 1st quartile: astrocytoma (HR=2.535, P=0.021), oligoastrocytoma (HR=4.169, P=0.014)
236 and glioblastoma multiforme (HR=2.163, P=0.042) (Table S3).
237
238 To evaluate the predictive performance of the signature, we employed receiver operating
239 characteristic (ROC) analyses and compared area under the curves (AUCs) derived from the

240 signature versus those derived from TNM staging. The signature had greater sensitivity and
241 specificity in predicting 5-year overall survival compared to TNM staging: papillary renal cell
242 (AUC=0.796 vs. AUC 0.640) and stomach (AUC=0.710 vs. AUC=0.561) (Fig. 3C). Importantly,
243 when used as a combined model with TNM staging, it outperformed either the signature or
244 TNM when considered alone, suggesting that incorporating molecular subtype information
245 on Notch-Hedgehog signalling allowed more precise stratification: clear cell renal cell
246 (AUC=0.802), papillary renal cell (AUC=0.812), liver (AUC=0.720) and stomach (AUC: 0.728)
247 (Fig. 3C). In terms of predicting prognosis in glioma subtypes, performance of the signature
248 was the best in oligoastrocytoma (AUC=0.823), followed by glioblastoma multiforme.
249 (AUC=0.761) and astrocytoma (AUC=0.743) (Fig. 3C). The signature also performed well when
250 all glioma subtypes were considered as a group (AUC=0.815) (Fig. 3C).
251
252
253 The Notch-Hedgehog signature identifies molecular subtypes with stem cell-like features
254
255 Notch-Hedgehog hyperactivation is associated with increased mortality rates (Fig. 2, 3). To
256 further investigate the underlying biological consequences of augmented Notch-Hedgehog
257 signalling and how they lead to adverse outcomes, we performed differential expression
258 analyses on all transcripts comparing high- and low-risk patients as predicted by the 13-gene
259 signature. The liver cancer cohort had the highest number of differentially expressed genes
260 (DEGs): 3,015 genes ($-1.5 > \log_2$ fold change > 1.5; $P<0.01$) (Table S4). This was followed by
261 glioma (1,407 genes), stomach (906 genes), papillary renal cell (817 genes) and clear cell
262 renal cell (545 genes) carcinoma (Table S4). Despite having very different pathologies, there
263 was a great deal of DEG overlap between these cancers. 14 DEGs were found in all five

264 cancers, 164 DEGs were observed in at least four cancers and 470 DEGs in at least three
265 cancers (Fig. S3A), implying conserved biological roles of Notch-Hedgehog signalling in driving
266 disease progression.
267
268 KEGG pathway analyses on DEGs demonstrated enrichments of pathways involved in
269 regulating self-renewal and pluripotency, i.e. Wnt, TGF- β, MAPK, JAK-STAT and PPAR
270 signalling (Fig. 3D; Fig. S3B), suggesting that tumours with hyperactive Notch-Hedgehog
271 signalling were characterised by molecular footprints of stemness and that there was
272 significant crosstalk between Notch-Hedgehog and other pathways involved in controlling
273 tumour initiation(28,29). Additionally, Gene Ontology analyses revealed significant
274 enrichments of processes related to cell differentiation, cell proliferation, embryo
275 development and morphogenesis (Fig. 3D), supporting the hypothesis that tumour
276 aggression and elevated mortality could be caused by the presence of cancer stem cells
277 (CSCs) that are likely to be refractory to therapy. Consistent with these results, Enrichr
278 transcription factor (TF) analyses revealed that TFs associated with stem cell function
279 appeared amongst top enriched candidates (Fig. 3D). DEGs were enriched as binding targets
280 of SUZ12, REST, EZH2, SMAD4 and FOXM1 as supported by both ChEA and ENCODE
281 databases (Fig. 3D). Binding targets of SUZ12 and EZH2 were consistently enriched across all
282 five cancer types, while targets of REST and SMAD4 were enriched in all cancers except for
283 clear cell renal cell carcinoma (Fig. 3D). These TFs were thought to induce epithelial-
284 mesenchymal transition and promote invasion and metastasis consistent with their roles in
285 tumour initiation and maintenance(30–32).
286

287 To independently confirm that the 13-gene signature is a potential pan-cancer marker of
288 CSCs, we performed Spearman's correlation analyses to compare 13-gene scores with
289 expression profiles of other CSC markers where we would expect to see positive correlations.
290 We examined expression profiles of nine genes implicated in CSC regulation: *CD105, CD133,*
291 *CD200, CD24, CD29, CD44, CD73, CD90* and *NESTIN*. Putative neural CSC markers are *CD133,*
292 *NESTIN, CD105* and *CD44*(33). We observed significant positive correlations between 13-gene
293 scores and all four markers in glioma samples (Fig. S4). *CD105, CD29, CD44, CD73, CD90* and
294 *NESTIN* were positively correlated with 13-gene scores in renal cancers (Fig. S4); an
295 observation which is consistent with these genes being markers of renal CSCs(34). Seven and
296 four CSC markers were positively correlated with 13-gene scores in liver and stomach cancers
297 respectively (Fig. S4). Given the tissue-specific nature of these genes, we would not expect to
298 see positive correlations in all cases. Nonetheless, our results overall suggest that hyperactive
299 Notch-Hedgehog signalling is associated with CSC phenotypes, contributing to tumour
300 aggression and poor survival outcomes.
301
302
303 **Transcription factors involved in self-renewal processes influence survival outcomes in patients**
304 **with hyperactive Notch-Hedgehog signalling**
305
306 Previously, we observed that binding targets of TFs associated with stem cell function were
307 enriched amongst DEGs (Fig. 3D). Polycomb proteins, EZH2 and SUZ12 have been implicated
308 in CSC formation and maintenance(35,36). REST is a transcriptional repressor involved in
309 maintaining embryonic and neural stem cell phenotypes(37). Given their roles in CSC
310 maintenance, we would expect to see elevated expression of these TFs in tumours with

311 hyperactive Notch-Hedgehog signalling. Indeed, we observed significant positive correlations
312 between 13-gene scores and *EZH2* levels in glioma (rho=0.45; P<0.0001), clear cell renal cell
313 (rho=0.22; P<0.0001), papillary renal cell (rho=0.33; P<0.0001) and liver (rho=0.26; P<0.0001)
314 cancers (Fig. 4A). Additionally, in the glioma cohort, positive associations between 13-gene
315 scores and *REST* (rho=0.39; P<0.0001) or *SUZ12* (rho=0.17; P<0.0001) profiles were observed
316 (Fig. 4D).
317
318 To determine whether these associations harboured prognostic information, patients were
319 categorised by their 13-gene scores and expression profiles of individual TFs into four
320 categories: *1)* high 13-gene score and high TF expression, *2)* high 13-gene score and low TF
321 expression, *3)* low 13-gene score and high TF expression and *4)* low 13-gene score and low TF
322 expression (Fig. 4A and 4D). Interestingly, combined relationship of the signature and TF
323 expression profiles allowed further delineation of patients into additional risk groups: glioma
324 (*EZH2*: P<0.0001; *REST*: P<0.0001 and *SUZ12*: P<0.0001), clear cell renal cell (*EZH2*:
325 P<0.0001), papillary renal cell (*EZH2*: P=0.029) and liver (*EZH2*: P<0.00057) cancers (Fig. 4B
326 and 4E). Patients with high 13-gene scores that concurrently harboured high TF expression
327 had the poorest survival outcomes: glioma (*EZH2*: HR=5.141, P<0.0001; *REST*: HR=3.646,
328 P<0.0001; *SUZ12*: HR=3.596, P<0.0001), clear cell renal cell (*EZH2*: HR=2.854, P<0.0001),
329 papillary renal cell (*EZH2*: HR=4.391, P=0.0099) and liver (*EZH2*: HR=2.685, P=0.0005) cancers
330 (Fig. 4C and 4F). Taken together, our results suggest that coregulation by Notch-Hedgehog
331 signalling and CSC TFs could synergistically contribute to more advanced disease states.
332
333
334 **Tumour hypoxia exacerbates disease phenotypes in Notch-Hedgehog^{+} CSCs**

335

336 Hypoxia is intricately linked to pluripotency as it promotes stem cell maintenance and self-
337 renewal in both embryonic stem cells and CSCs(38), in part, through modulating hypoxia-
338 inducible factor (HIF) function(39). For example, glioma stem cells are typically found in the
339 vicinity of necrotic regions that are hypoxic(40). Glioma stem cells have increased ability to
340 stimulate angiogenesis through VEGF upregulation(41) and inhibition of HIFs could reduce
341 CSC survival, self-renewal and proliferation(40). We reason that hypoxia functions to
342 maintain CSC niches. To assess the levels of tumour hypoxia, we employed a 52-hypoxia gene
343 signature(17) for calculating hypoxia scores in each patient by taking the average expression
344 of hypoxia signature genes(17). Indeed, we observed significant positive correlations
345 between Notch-Hedgehog^{+} CSCs and hypoxia scores in glioma (rho=0.33, P<0.0001) and clear
346 cell renal cell carcinoma (rho=0.16, P=0.00031) (Fig. 5A). By grouping patients based on their
347 13-gene and hypoxia scores, this joint model allowed the identification of patients with
348 potentially more hypoxic tumours harbouring Notch-Hedgehog^{+} CSCs, which influenced
349 overall survival rates: glioma (P<0.0001) and clear cell renal cell carcinoma (P=0.00013) (Fig.
350 5B). Indeed, patients with high CSC and hypoxia scores had significantly poorer survival
351 outcomes: glioma (HR=6.008; P<0.0001) and clear cell renal cell carcinoma (HR=2.389,
352 P<0.0001) (Fig. 5C). The CSC-hypoxia model is also prognostic in glioma subtypes:
353 astrocytoma (HR=5.052, P<0.0001), oligoastrocytoma (HR=16.717, P=0.0066) and
354 glioblastoma (HR=2.686, P=0.022) (Fig. 5B and 5C). Our results suggest that hypoxic zones
355 within tumours could very well represent CSC niches.

356

357

358 **Putative Notch-Hedgehog^{+} CSCs are potentially immune privileged**

359

360 Cancer progression is negatively correlated with immunocompetence of the host and
361 evidence points to the role of CSCs in immunomodulation(3,42). CSCs reside within niches
362 that are often protected from environmental insults as well as attacks by the immune
363 system. Hypoxic zones not only serve as CSC niches (Fig. 5)(43), but also attract
364 immunosuppressive cells such as regulatory T cells (Tregs)(22,44), tumour-associated
365 macrophages(45) and myeloid-derived suppressor cells(46). Given that positive associations
366 between Notch-Hedgehog^{+} CSCs and hypoxia were linked to poor progression in glioma and
367 clear cell renal cell carcinoma, we hypothesize that tumours characterised by these features
368 would be immune privileged or hypoimmunogenic.

369

370 To test this hypothesis, we retrieved a list of 31 genes that represent tumour-infiltrating
371 Tregs. This gene list was identified from the overlap of four Treg signatures(18–21) to yield a
372 more representative profile of tumour-infiltrating Tregs that is not specific to a single cancer
373 type. A Treg score for each patient within the glioma and clear cell renal cell carcinoma
374 cohorts was calculated as the mean expression of the 31 genes. We observed significant
375 positive correlations between Treg scores and the Notch-Hedgehog 13-gene scores in both
376 cohorts, supporting the hypothesis that CSCs are potentially hypoimmunogenic: glioma
377 (rho=0.43; P<0.0001) and clear cell renal cell carcinoma (rho=0.31; P<0.0001) (Fig. 6A). As
378 performed previously, patients were separated into four groups based on their 13-gene and
379 Treg scores. When used in combination with the Notch-Hedgehog signature, Treg expression
380 profiles allowed further separation of patients into additional risk groups that influenced
381 overall survival: glioma (P<0.0001) and clear cell renal cell carcinoma (P<0.0001) (Fig. 6B).
382 Intriguingly, patients characterised by high 13-gene and Treg scores had significantly higher

383 mortality rates compared to those with low 13-gene and Treg scores: glioma (HR=4.921,
384 P<0.0001) and clear cell renal cell carcinoma (HR=2.968, P<0.0001) (Fig. 6C). This was also
385 true for other histological subtypes of glioma: astrocytoma (HR=2.721; P=0.0032),
386 oligoastrocytoma (HR=5.431; P=0.0091) and glioblastoma (HR=3.065; P=0.0068) (Fig. 6C).
387 Taken together, our results suggest that CSCs found within immunosuppressed environments
388 are likely to be more aggressive.

389 Discussion and Conclusion:

390

391 Aberrations in the Notch-Hedgehog signalling axis are frequently implicated in malignant
392 progression. Hedgehog genes, *Shh, PTCH1* and *GLI1*, were detected in over 50% of liver
393 cancer tumours and inhibition of Hedgehog signalling by cyclopamine, Smoothened
394 antagonist or anti-SHH resulted in decreased cell growth and increased apoptosis(47). Notch
395 signalling is also activated in liver cancer and this leads to formation of liver tumours in
396 mice(48). Notch blockade using γ-secretase inhibitors reduced cell viability in hepatoma cell
397 lines(48). In clear cell renal cell carcinoma, inhibition of Notch signalling reduced anchorage-
398 independent growth and mice treated with Notch inhibitors had impaired growth of
399 transplanted cancer cells(49). Elevated expression of Notch ligands correlated with
400 aggressiveness and poor survival rates in stomach cancer(50).

401

402 These studies have paved the road for understanding the role of Notch-Hedgehog signalling
403 in carcinogenesis. However, large-scale comparative studies investigating the similarities and
404 differences in Notch-Hedgehog signalling across multiple cancer types have remained limited.
405 We interrogated expression and mutational profiles of 72 genes from Notch and Hedgehog
406 pathways in 21 diverse cancer types involving 18,484 patients. Our integrated analysis of
407 genomic, transcriptomic and clinical data revealed molecular distinct tumour subtypes that
408 were characterised by Notch-Hedgehog hyperactivation. Concentrating on 13 Notch-
409 Hedgehog driver genes that were recurrently amplified and overexpressed, we found that
410 these genes were associated with clinically relevant molecular features of stemness. The
411 biological consequences of elevated expression of driver genes were manifold. High-risk
412 patients showed overexpression of genes associated with other stem cell-related pathways

413 such as Wnt, JAK-STAT and TGF-β signalling (Fig. 3D. and S3B)(51). Simultaneous inhibition of
414 Notch and JAK-STAT pathways by combined AG-490 and GSI IX therapy impaired pancreatic
415 cancer progression(52). *GLI2* is regulated by both Hedgehog and TGF-β pathways and others
416 have surmised that TGF-β may potentiate Hedgehog signalling cascade by increasing *GL12*
417 availability, contributing to metastasis(53). Hence, our study reveals molecular targets with
418 overlapping functions that can be prioritised to improve therapeutic outcomes.
419
420 Furthermore, binding targets of stem cell-related TFs (*EZH2, SUZ12* and *REST*) were enriched
421 amongst genes upregulated in high-risk patients (Fig. 4). *EZH2* synergises with Notch-
422 Hedgehog^{+} CSCs to worsen survival outcomes in patients with glioma, renal and liver cancers
423 (Fig. 4). Pharmacological inhibition of *EZH2* impaired glioblastoma CSC tumour-initiating
424 capacity and survival(35). *EZH2*-mediated transcriptional silencing leads to the maintenance
425 of undifferentiated states in glioblastoma through *STAT3* activation(54). In liver cancer, *EZH2*
426 overexpression is associated with vascular invasion, malignant progression(55) and activation
427 of β-catenin/Wnt signalling(56). Inhibition of *EZH2* in renal cancer cell lines led to increased
428 apoptosis(57). Additionally, enrichments of *SUZ12* and *REST* targets in glioma patients with
429 hyperactive Notch-Hedgehog signalling were linked to significantly poorer prognosis (Fig. 4D
430 and 4E). *REST* is implicated in transcriptional regulation of neuronal stem cells(37), while the
431 overexpression of *SUZ12* is linked to tumour progression(58).
432
433 An exploration of the relationship between Notch-Hedgehog hyperactivation and tumour
434 microenvironmental qualities revealed associations of CSCs with hypoxia and
435 immunosuppression. We observed that CSCs characterised by hyperactive Notch-Hedgehog
436 signalling exhibited immune privileged features associated with the attenuation effects of

437 Tregs (Fig. 6). Effectiveness of immunotherapy is biased towards differentiated cells that
438 make up the tumour bulk due to distinct antigen presentation in CSCs(59). CD133^{+} glioma
439 CSCs fail to express NK cell ligands or MHCI, which prevents immune detection(60).
440 Stimulatory NK cell ligands are also downregulated in breast CSCs, contributing to evasion
441 from NK cell killing(61). Pan et al. elegantly reviewed recent initiatives focusing on
442 immunotherapeutic agents against CSC antigens employing dendritic cell vaccines, myeloid-
443 derived suppressor cell-based approaches and the use of immune checkpoint blockades
444 recognising *PD-1* or *CTLA4*(59). The Notch-Hedgehog signature may be used to stratify
445 patients prior to immunotherapy.
446
447 Immunoevasion can be exacerbated by tumour hypoxia as the latter not only promotes CSC
448 survival, but also creates an environment that facilitates further immune suppression(22). It
449 may be possible that Notch-Hedgehog^{+} CSCs in glioma and clear cell renal cell carcinomas are
450 more frequently found within immunosuppressed hypoxic zones (Fig. 5). Indeed, hypoxia
451 could stimulate self-renewal of CD133^{+} glioma stem cells and this is abrogated by HIF-1α
452 knockdown(62). Hypoxia promotes the maintenance of undifferentiated states through the
453 activation of Notch-responsive genes in neuronal progenitors(39). Hypoxia also activates
454 cellular reprogramming of non-stem cancer cells into CSCs in glioblastoma by inducing the
455 expression of *Oct4, Nanog* and *c-Myc*(63). Glioma stem cells are pro-angiogenic due to
456 promiscuous secretions of VEGF that is further induced by hypoxia(41). Bevacizumab, which
457 targets VEGF, could suppress xenographs derived from glioma stem cells but not those
458 derived from non-stem glioma cells(41). In renal cancer, we observed that Notch-Hedgehog^{+}
459 CSCs are likely to be enriched in hypoxic tumours and the combined effects of hypoxia and
460 augmented Notch-Hedgehog signalling resulted in further elevation of death risks (Fig. 5).

461 However, Sjölund et al. observed that Notch signalling is not enhanced by hypoxia in renal
462 cancer(49). Another study on renal CSCs revealed that hypoxia did not affect the
463 differentiation potential of $CD105^+$ CSCs(64). Nonetheless, hypoxia was found to induce the
464 expression of stem cell markers, *Oct4, Nanog, c-Myc* and *Klf4* in renal cancer cell lines,
465 supporting our observation, and in another ten cancers including cervix, lung, colon, liver and
466 prostate(65).
467
468 Although prospective validation is warranted, the results presented in this work support a
469 model where Notch-Hedgehog hyperactivation is linked to stemness and that hypoxia
470 contributes to the maintenance of undifferentiated phenotypes and the reduction of anti-
471 tumour immunity. The use of immune checkpoint blockade has been increasingly tried in
472 malignancy(66). Hence, molecular signatures capable of discerning responders from non-
473 responders will be valuable prior to the administration of these expensive drugs. As an
474 independent prognostic indicator in five cancer types involving 2,278 patients, the Notch-
475 Hedgehog gene signature may serve as a staging point for exploring combinatorial
476 treatments that simultaneously target CSCs, hypoxia and tumour immunity.
477

Additional Information

Ethics approval and consent to participate: No ethics approval or consent to participate is required as this study is conducted using publicly available datasets from The Cancer Genome Atlas.

Consent for publication: Not applicable.

Availability of data and material: The datasets supporting the conclusions of this article are included within the article and its supplementary files.

Conflict of interest: None declared.

Funding: None.

Authors' contributions: AGL designed the study and supervised the research. WHC and AGL analysed the data, interpreted the results and wrote the initial manuscript draft. AGL revised the manuscript draft. All authors approved the final submitted manuscript.

Acknowledgements: None.

499 References:

500

501 1. Maugeri-Saccà M, Bartucci M, De Maria R. DNA damage repair pathways in cancer

502 stem cells. Mol Cancer Ther. 2012;11(8):1627–36.

503 2. Chang WH, Lai AG. Transcriptional landscape of DNA repair genes underpins a pan-

504 cancer prognostic signature associated with cell cycle dysregulation and tumor

505 hypoxia. DNA Repair (Amst) [Internet]. 2019 Jun;78:142–53. Available from:

506 http://www.ncbi.nlm.nih.gov/pubmed/31054516

507 3. Schatton T, Frank MH. Antitumor immunity and cancer stem cells. Ann N Y Acad Sci.

508 2009;1176(1):154–69.

509 4. Clevers H. The cancer stem cell: premises, promises and challenges. Nat Med.

510 2011;17(3):313.

511 5. Takebe N, Harris PJ, Warren RQ, Ivy SP. Targeting cancer stem cells by inhibiting Wnt,

512 Notch, and Hedgehog pathways. Nat Rev Clin Oncol. 2011;8(2):97.

513 6. Ellisen LW, Bird J, West DC, Soreng AL, Reynolds TC, Smith SD, et al. TAN-1, the human

514 homolog of the Drosophila notch gene, is broken by chromosomal translocations in T

515 lymphoblastic neoplasms. Cell. 1991;66(4):649–61.

516 7. Lobry C, Oh P, Aifantis I. Oncogenic and tumor suppressor functions of Notch in

517 cancer: it's NOTCH what you think. J Exp Med. 2011;208(10):1931–5.

518 8. Briscoe J, Thérond PP. The mechanisms of Hedgehog signalling and its roles in

519 development and disease. Nat Rev Mol cell Biol. 2013;14(7):416.

520 9. Solecki DJ, Liu X, Tomoda T, Fang Y, Hatten ME. Activated Notch2 signaling inhibits

521 differentiation of cerebellar granule neuron precursors by maintaining proliferation.

522 Neuron. 2001;31(4):557–68.

523 10. Dakubo GD, Mazerolle CJ, Wallace VA. Expression of Notch and Wnt pathway
524 components and activation of Notch signaling in medulloblastomas from heterozygous
525 patched mice. J Neurooncol. 2006;79(3):221–7.
526 11. Katoh M. Networking of WNT, FGF, Notch, BMP, and Hedgehog signaling pathways
527 during carcinogenesis. Stem Cell Rev. 2007;3(1):30–8.
528 12. Steg AD, Katre AA, Goodman BW, Han H-D, Nick AM, Stone RL, et al. Targeting the
529 notch ligand JAGGED1 in both tumor cells and stroma in ovarian cancer. Clin cancer
530 Res. 2011;clincanres--0432.
531 13. Domingo-Domenech J, Vidal SJ, Rodriguez-Bravo V, Castillo-Martin M, Quinn SA,
532 Rodriguez-Barrueco R, et al. Suppression of acquired docetaxel resistance in prostate
533 cancer through depletion of notch-and hedgehog-dependent tumor-initiating cells.
534 Cancer Cell. 2012;22(3):373–88.
535 14. Schreck KC, Taylor P, Marchionni L, Gopalakrishnan V, Bar EE, Gaiano N, et al. The
536 Notch target Hes1 directly modulates Gli1 expression and Hedgehog signaling: a
537 potential mechanism of therapeutic resistance. Clin cancer Res. 2010;16(24):6060–70.
538 15. Weinstein JN, Collisson EA, Mills GB, Shaw KRM, Ozenberger BA, Ellrott K, et al. The
539 cancer genome atlas pan-cancer analysis project. Nat Genet. 2013;45(10):1113.
540 16. Mermel CH, Schumacher SE, Hill B, Meyerson ML, Beroukhim R, Getz G. GISTIC2. 0
541 facilitates sensitive and confident localization of the targets of focal somatic copy-
542 number alteration in human cancers. Genome Biol. 2011;12(4):R41.
543 17. Buffa FM, Harris AL, West CM, Miller CJ. Large meta-analysis of multiple cancers
544 reveals a common, compact and highly prognostic hypoxia metagene. Br J Cancer
545 [Internet]. 2010;102(2):428–35. Available from:
546 http://dx.doi.org/10.1038/sj.bjc.6605450

547 18. Zheng C, Zheng L, Yoo JK, Guo H, Zhang Y, Guo X, et al. Landscape of Infiltrating T Cells
548 in Liver Cancer Revealed by Single-Cell Sequencing. Cell [Internet]. 2017;169(7):1342-
549 1356.e16. Available from: http://dx.doi.org/10.1016/j.cell.2017.05.035
550 19. De Simone M, Arrigoni A, Rossetti G, Gruarin P, Ranzani V, Politano C, et al.
551 Transcriptional Landscape of Human Tissue Lymphocytes Unveils Uniqueness of
552 Tumor-Infiltrating T Regulatory Cells. Immunity [Internet]. 2016;45(5):1135–47.
553 Available from: http://dx.doi.org/10.1016/j.immuni.2016.10.021
554 20. Plitas G, Konopacki C, Wu K, Bos PD, Morrow M, Putintseva E V, et al. Regulatory T
555 cells exhibit distinct features in human breast cancer. Immunity. 2016;45(5):1122–34.
556 21. Tirosh I, Izar B, Prakadan SM, Wadsworth MH, Treacy D, Trombetta JJ, et al. Dissecting
557 the multicellular ecosystem of metastatic melanoma by single-cell RNA-seq. Science
558 (80-). 2016;352(6282):189–96.
559 22. Chang WH, Forde D, Lai AG. A novel signature derived from immunoregulatory and
560 hypoxia genes predicts prognosis in liver and five other cancers. J Transl Med
561 [Internet]. 2019 Jan 9;17(1):14. Available from:
562 http://www.ncbi.nlm.nih.gov/pubmed/30626396
563 23. Chang WH, Forde D, Lai AG. Dual prognostic role for 2-oxoglutarate oxygenases in ten
564 diverse cancer types: Implications for cell cycle regulation and cell adhesion
565 maintenance. Cancer Commun. 2019;39(23).
566 24. Chang WH, Lai AG. Timing gone awry: distinct tumour suppressive and oncogenic roles
567 of the circadian clock and crosstalk with hypoxia signalling in diverse malignancies. J
568 Transl Med [Internet]. 2019 Apr 23;17(1):132. Available from:
569 https://www.biorxiv.org/content/early/2019/02/21/556878
570 25. Tabas-Madrid D, Nogales-Cadenas R, Pascual-Montano A. GeneCodis3: a non-

571 redundant and modular enrichment analysis tool for functional genomics. Nucleic
572 Acids Res. 2012;40(W1):W478--W483.
573 26. Kuleshov M V, Jones MR, Rouillard AD, Fernandez NF, Duan Q, Wang Z, et al. Enrichr: a
574 comprehensive gene set enrichment analysis web server 2016 update. Nucleic Acids
575 Res. 2016;44(W1):W90--W97.
576 27. Haider S, McIntyre A, van Stiphout RGPM, Winchester LM, Wigfield S, Harris AL, et al.
577 Genomic alterations underlie a pan-cancer metabolic shift associated with tumour
578 hypoxia. Genome Biol. 2016;17(1):1–17.
579 28. Chang WH, Lai AG. An immunoevasive strategy through clinically-relevant pan-cancer
580 genomic and transcriptomic alterations of JAK-STAT signaling components. bioRxiv
581 [Internet]. 2019; Available from:
582 https://www.biorxiv.org/content/early/2019/03/14/576645
583 29. Chang WH, Lai AG. The pan-cancer mutational landscape of the PPAR pathway reveals
584 universal patterns of dysregulated metabolism and interactions with tumor immunity
585 and hypoxia. Ann N Y Acad Sci [Internet]. 2019 Jul;1448(1):65–82. Available from:
586 https://www.biorxiv.org/content/early/2019/02/28/563676
587 30. Bao B, Wang Z, Ali S, Kong D, Banerjee S, Ahmad A, et al. Over-expression of FoxM1
588 leads to epithelial--mesenchymal transition and cancer stem cell phenotype in
589 pancreatic cancer cells. J Cell Biochem. 2011;112(9):2296–306.
590 31. Zingg D, Debbache J, Schaefer SM, Tuncer E, Frommel SC, Cheng P, et al. The
591 epigenetic modifier EZH2 controls melanoma growth and metastasis through silencing
592 of distinct tumour suppressors. Nat Commun. 2015;6:6051.
593 32. Li H, Cai Q, Wu H, Vathipadiekal V, Dobbin ZC, Li T, et al. SUZ12 promotes human
594 epithelial ovarian cancer by suppressing apoptosis via silencing HRK. Mol Cancer Res.

595 2012;
596 33. Hovinga KE, Shimizu F, Wang R, Panagiotakos G, Van Der Heijden M, Moayedpardazi H,
597 et al. Inhibition of notch signaling in glioblastoma targets cancer stem cells via an
598 endothelial cell intermediate. Stem Cells. 2010;28(6):1019–29.
599 34. Bussolati B, Dekel B, Azzarone B, Camussi G. Human renal cancer stem cells. Cancer
600 Lett. 2013;338(1):141–6.
601 35. Suvà M-L, Riggi N, Janiszewska M, Radovanovic I, Provero P, Stehle J-C, et al. EZH2 is
602 essential for glioblastoma cancer stem cell maintenance. Cancer Res. 2009;8–5472.
603 36. Sauvageau M, Sauvageau G. Polycomb group proteins: multi-faceted regulators of
604 somatic stem cells and cancer. Cell Stem Cell. 2010;7(3):299–313.
605 37. Johnson R, Teh CH, Kunarso G, Wong KY, Srinivasan G, Cooper ML, et al. REST
606 regulates distinct transcriptional networks in embryonic and neural stem cells. PLoS
607 Biol. 2008;6(10):e256.
608 38. Keith B, Simon MC. Hypoxia-inducible factors, stem cells, and cancer. Cell.
609 2007;129(3):465–72.
610 39. Gustafsson M V, Zheng X, Pereira T, Gradin K, Jin S, Lundkvist J, et al. Hypoxia requires
611 notch signaling to maintain the undifferentiated cell state. Dev Cell. 2005;9(5):617–28.
612 40. Li Z, Bao S, Wu Q, Wang H, Eyler C, Sathornsumetee S, et al. Hypoxia-inducible factors
613 regulate tumorigenic capacity of glioma stem cells. Cancer Cell. 2009;15(6):501–13.
614 41. Bao S, Wu Q, Sathornsumetee S, Hao Y, Li Z, Hjelmeland AB, et al. Stem cell--like
615 glioma cells promote tumor angiogenesis through vascular endothelial growth factor.
616 Cancer Res. 2006;66(16):7843–8.
617 42. Kawasaki BT, Farrar WL. Cancer stem cells, CD200 and immunoevasion. Trends
618 Immunol. 2008;29(10):464–8.

619 43. Ledaki I, McIntyre A, Wigfield S, Buffa F, McGowan S, Baban D, et al. Carbonic
620 anhydrase IX induction defines a heterogeneous cancer cell response to hypoxia and
621 mediates stem cell-like properties and sensitivity to HDAC inhibition. Oncotarget
622 [Internet]. 2015;6(23). Available from: http://www.oncotarget.com/fulltext/4989
623 44. Clambey ET, McNamee EN, Westrich JA, Glover LE, Campbell EL, Jedlicka P, et al.
624 Hypoxia-inducible factor-1 alpha--dependent induction of FoxP3 drives regulatory T-
625 cell abundance and function during inflammatory hypoxia of the mucosa. Proc Natl
626 Acad Sci. 2012;201202366.
627 45. Doedens AL, Stockmann C, Rubinstein MP, Liao D, Zhang N, DeNardo DG, et al.
628 Macrophage expression of hypoxia-inducible factor-1α suppresses T-cell function and
629 promotes tumor progression. Cancer Res. 2010;8–5472.
630 46. Noman MZ, Hasmim M, Messai Y, Terry S, Kieda C, Janji B, et al. Hypoxia: a key player
631 in antitumor immune response. A Review in the Theme: Cellular Responses to Hypoxia.
632 Am J Physiol - Cell Physiol [Internet]. 2015;309(9):C569–79. Available from:
633 http://ajpcell.physiology.org/lookup/doi/10.1152/ajpcell.00207.2015
634 47. Huang S, He J, Zhang X, Bian Y, Yang L, Xie G, et al. Activation of the hedgehog pathway
635 in human hepatocellular carcinomas. Carcinogenesis. 2006;27(7):1334–40.
636 48. Villanueva A, Alsinet C, Yanger K, Hoshida Y, Zong Y, Toffanin S, et al. Notch signaling is
637 activated in human hepatocellular carcinoma and induces tumor formation in mice.
638 Gastroenterology. 2012;143(6):1660–9.
639 49. Sjölund J, Johansson M, Manna S, Norin C, Pietras A, Beckman S, et al. Suppression of
640 renal cell carcinoma growth by inhibition of Notch signaling in vitro and in vivo. J Clin
641 Invest. 2008;118(1):217–28.
642 50. Yeh T-S, Wu C-W, Hsu K-W, Liao W-J, Yang M-C, Li AF-Y, et al. The activated Notch1

643 signal pathway is associated with gastric cancer progression through cyclooxygenase-
644 2. Cancer Res. 2009;69(12):5039–48.
645 51. Chang WH, Lai AG. Pan-cancer genomic amplifications underlie a Wnt hyperactivation
646 phenotype associated with stem cell-like features leading to poor prognosis. Transl
647 Res. 2019;
648 52. Palagani V, Bozko P, El Khatib M, Belahmer H, Giese N, Sipos B, et al. Combined
649 inhibition of Notch and JAK/STAT is superior to monotherapies and impairs pancreatic
650 cancer progression. Carcinogenesis. 2013;35(4):859–66.
651 53. Javelaud D, Alexaki VI, Dennler S, Mohammad KS, Guise TA, Mauviel A. TGF-
652 β/SMAD/GLI2 signaling axis in cancer progression and metastasis. Cancer Res.
653 2011;71(17):5606–10.
654 54. Kim E, Kim M, Woo D-H, Shin Y, Shin J, Chang N, et al. Phosphorylation of EZH2
655 activates STAT3 signaling via STAT3 methylation and promotes tumorigenicity of
656 glioblastoma stem-like cells. Cancer Cell. 2013;23(6):839–52.
657 55. Sasaki M, Ikeda H, Itatsu K, Yamaguchi J, Sawada S, Minato H, et al. The overexpression
658 of polycomb group proteins Bmi1 and EZH2 is associated with the progression and
659 aggressive biological behavior of hepatocellular carcinoma. Lab Investig.
660 2008;88(8):873.
661 56. Cheng ASL, Lau SS, Chen Y, Kondo Y, Li MS, Feng H, et al. EZH2-mediated concordant
662 repression of Wnt antagonists promotes β-catenin--dependent hepatocarcinogenesis.
663 Cancer Res. 2011;
664 57. Wagener N, Macher-Goeppinger S, Pritsch M, Hüsing J, Hoppe-Seyler K, Schirmacher
665 P, et al. Enhancer of zeste homolog 2 (EZH2) expression is an independent prognostic
666 factor in renal cell carcinoma. BMC Cancer. 2010;10(1):524.

667 58. Zhang J, Wu W, Xu S, Zhang J, Zhang J, Yu Q, et al. MicroRNA-105 inhibits human
668 glioma cell malignancy by directly targeting SUZ12. Tumor Biol.
669 2017;39(6):1010428317705766.
670 59. Pan Q, Li Q, Liu S, Ning N, Zhang X, Xu Y, et al. Concise review: targeting cancer stem
671 cells using immunologic approaches. Stem Cells. 2015;33(7):2085–92.
672 60. Wu A, Wiesner S, Xiao J, Ericson K, Chen W, Hall WA, et al. Expression of MHC I and NK
673 ligands on human CD133+ glioma cells: possible targets of immunotherapy. J
674 Neurooncol. 2007;83(2):121–31.
675 61. Wang B, Wang Q, Wang Z, Jiang J, Yu S-C, Ping Y-F, et al. Metastatic consequences of
676 immune escape from NK cell cytotoxicity by human breast cancer stem cells. Cancer
677 Res. 2014;
678 62. Soeda A, Park M, Lee D, Mintz A, Androutsellis-Theotokis A, McKay RD, et al. Hypoxia
679 promotes expansion of the CD133-positive glioma stem cells through activation of HIF-
680 1α. Oncogene. 2009;28(45):3949.
681 63. Heddleston JM, Li Z, McLendon RE, Hjelmeland AB, Rich JN. The hypoxic
682 microenvironment maintains glioblastoma stem cells and promotes reprogramming
683 towards a cancer stem cell phenotype. Cell cycle. 2009;8(20):3274–84.
684 64. Azzi S, Bruno S, Giron-Michel J, Clay D, Devocelle A, Croce M, et al. Differentiation
685 therapy: targeting human renal cancer stem cells with interleukin 15. J Natl Cancer
686 Inst. 2011;103(24):1884–98.
687 65. Mathieu J, Zhang Z, Zhou W, Wang AJ, Heddleston JM, Pinna CMA, et al. HIF induces
688 human embryonic stem cell markers in cancer cells. Cancer Res. 2011;
689 66. Topalian SL, Drake CG, Pardoll DM. Immune checkpoint blockade: a common
690 denominator approach to cancer therapy. Cancer Cell. 2015;27(4):450–61.

691

692

693

694 Figure Legends:

695

696 **Figure 1. Pan-cancer drivers of Notch-Hedgehog signalling. (A)** Schematic diagram illustrating
697 the study design and the identification of Notch-Hedgehog driver genes, which represent the
698 13-gene signature. SCNA and expression profiles of 72 Notch-Hedgehog pathway genes were
699 interrogated in 21 cancer types involving 18,484 patients. We identified 70 genes as
700 amplified in at least 20% of samples and 35 genes that were amplified in at least 20% of
701 samples in at least 7 cancer types. Differential expression analyses between tumour and non-
702 tumour samples revealed that the 13 recurrently amplified genes were also upregulated,
703 potentially indicating a gain-of-function. These 13 genes were prioritised as a Notch-
704 Hedgehog signature, which was prognostic in five cancer types involving 2,278 patients.
705 Associations of the signature with tumour microenvironmental features of hypoxia and
706 immunity were also investigated. Pie slices indicate the number of samples within each
707 cancer type. **(B)** Stacked bar graphs represent the proportion of samples in each cancer type
708 with SCNA of Hedgehog and Notch pathway genes. Width of the bars reflect the number of
709 samples within each cancer. **(C)** Somatic gains and differential expression profiles of 35
710 Notch-Hedgehog genes that were recurrently amplified in at least 7 cancer types (one-third
711 of all cancers). Cumulative bar charts on the left represent the number of cancers with at
712 least 20% of samples with somatic amplification. Heatmap on the left represents the extent
713 of somatic gains for each of the 35 genes separated into Hedgehog and Notch signalling
714 pathways across 21 cancers. Heatmap intensities depict the fraction of the cohort in which a
715 given gene is amplified. Columns (cancer types) were ordered using Euclidean distance
716 metric and hierarchical clustering to reveal cancers that were similar. Heatmap on the right
717 represents tumour and non-tumour differential expression values (log_2) for the 35 genes.

718 Genes highlighted in red represent the 13 Notch-Hedgehog signature genes. Cancer
719 abbreviations were listed in Table S2.
720
721 **Figure 2. The Notch-Hedgehog 13-gene signature predicts patient survival in five cancers. (A)**
722 Kaplan-Meier estimates for overall survival using the signature. Patients were ranked and
723 quartile stratified into Q1 (<25%), Q2 (25-50%), Q3 (50-75%) and Q4 (>75%) based on their
724 13-gene scores. P values were determined using the log-rank test. **(B)** Separation of tumour
725 from non-tumour samples using the signature. Ordination plots of MDS analysis of the
726 signature using Euclidean distances to represent tumour and non-tumour samples in 2-
727 dimensional space. PERMANOVA test confirmed statistically significant differences between
728 tumour and non-tumour samples.
729
730 **Figure 3. The Notch-Hedgehog 13-gene signature is independent of TNM stage and predicts**
731 **overall survival in glioma histological subtypes. (A)** Kaplan-Meier analyses were performed on
732 patients stratified according to TNM stages and 13-gene scores. Patients were first separated
733 into TNM stage and then median-stratified into low- and high-score groups based on their
734 13-gene scores. P values were determined using the log-rank test. **(B)** Kaplan-Meier estimates
735 for overall survival using the signature on glioma subtypes ranging from low-grade
736 (astrocytoma, oligoastrocytoma) to high-grade gliomas (glioblastoma multiforme). Patients
737 were first stratified by histological subtypes followed by quartile stratification into Q1 (<25%),
738 Q2 (25-50%), Q3 (50-75%) and Q4 (>75%) based on their 13-gene scores. P values were
739 determined using the log-rank test. **(C)** Predictive performance of the signature. The receiver
740 operating characteristic (ROC) analysis was used to assess specificity and sensitivity of the
741 signature in predicting 5-year overall survival. ROC curves generated from the signature were

742 compared to those generated from TNM staging and a combined model uniting TNM stage
743 and the signature. AUCs for TNM stage were in accordance with previous publications
744 employing TCGA datasets(2,22,51). AUC: area under the curve. TNM: tumour, node and
745 metastasis. **(D)** Enriched biological pathways and transcription factor binding associated with
746 DEGs. Differential expression analyses were performed between Q4 and Q1 patients
747 followed by mapping of DEGs against KEGG, Gene Ontology, ChEA and ENCODE databases.
748

749 **Figure 4. Prognostic significance of a combined model of the Notch-Hedgehog signature and**
750 **transcription factors (*EZH2, SUZ12* and *REST*) involved in pluripotency maintenance. (A)** Scatter
751 plots demonstrate significant positive correlations between 13-gene scores and *EZH2*
752 expression profiles in four cancers. Patients were stratified into four categories based on
753 median 13-gene scores and *EZH2* expression. Density plots depict the distribution of 13-gene
754 scores and *EZH2* expression at the y- and x-axes respectively. **(B)** Kaplan-Meier analyses were
755 performed on the four patient categories to ascertain the combined relationship of the
756 signature and *EZH2* expression on overall survival. **(C)** Table inset depicts univariate Cox
757 proportional hazards analyses of the relationship between *EZH2* and the signature in four
758 cancer types. **(D)** Scatter plots demonstrate significant positive correlations between 13-gene
759 scores and *REST* or *SUZ12* expression levels in glioma. Patients were stratified into four
760 categories based on median 13-gene score and *REST* or *SUZ12* expression. Density plots
761 depict the distribution of 13-gene scores and *REST* or *SUZ12* expression at the y- and x-axes
762 respectively. **(E)** Kaplan-Meier analyses were performed on the four patient categories to
763 ascertain the combined relationship between the signature and *REST* or *SUZ12* expression on
764 overall survival in glioma. **(F)** Table inset depicts univariate Cox proportional hazards analyses

765 of the relationship between *REST* or *SUZ12* and the signature in glioma. CI: confidence
766 interval. Significant P values are highlighted in bold.
767
768
769 **Figure 5. Positive associations between Notch-Hedgehog$^+$ CSCs and tumour hypoxia in glioma**
770 **and clear cell renal cell carcinoma. (A)** Scatter plots demonstrate significant positive
771 correlations between 13-gene and hypoxia scores. Patients were stratified into four
772 categories based on median 13-gene and hypoxia scores. Density plots depict the distribution
773 of 13-gene and hypoxia scores at the y- and x-axes respectively. **(B)** Kaplan-Meier analyses
774 were performed on the four patient categories to ascertain the combined relationship of the
775 signature and tumour hypoxia on overall survival. Contribution of hypoxia on Notch-
776 Hedgehog$^+$ CSCs were also determined in histological subtypes of glioma (astrocytoma,
777 oligoastrocytoma and glioblastoma multiforme). **(C)** Table inset demonstrates univariate Cox
778 proportional hazards analyses of the relationship between tumour hypoxia and the signature
779 in glioma and clear cell renal cell carcinoma. CI: confidence interval. Significant P values are
780 highlighted in bold.
781
782
783 **Figure 6. Positive associations between Notch-Hedgehog$^+$ CSCs and immunosuppression in**
784 **glioma and clear cell renal cell carcinoma. (A)** Scatter plots demonstrate significant positive
785 correlations between 13-gene and Treg scores. Patients were stratified into four categories
786 based on median 13-gene and Treg scores. Density plots depict the distribution of 13-gene
787 and Treg scores at the y- and x-axes respectively. **(B)** Kaplan-Meier analyses were performed
788 on the four patient categories to ascertain the combined relationship of the signature and

789 Treg-mediated immunosuppression on overall survival. Contribution of Tregs on Notch-
790 Hedgehog^{+} CSCs were also determined in histological subtypes of glioma (astrocytoma,
791 oligoastrocytoma and glioblastoma multiforme). **(C)** Table inset demonstrates univariate Cox
792 proportional hazards analyses of the relationship between Tregs and the signature in glioma
793 and clear cell renal cell carcinoma. CI: confidence interval. Significant P values are highlighted
794 in bold.
795

Figure 1

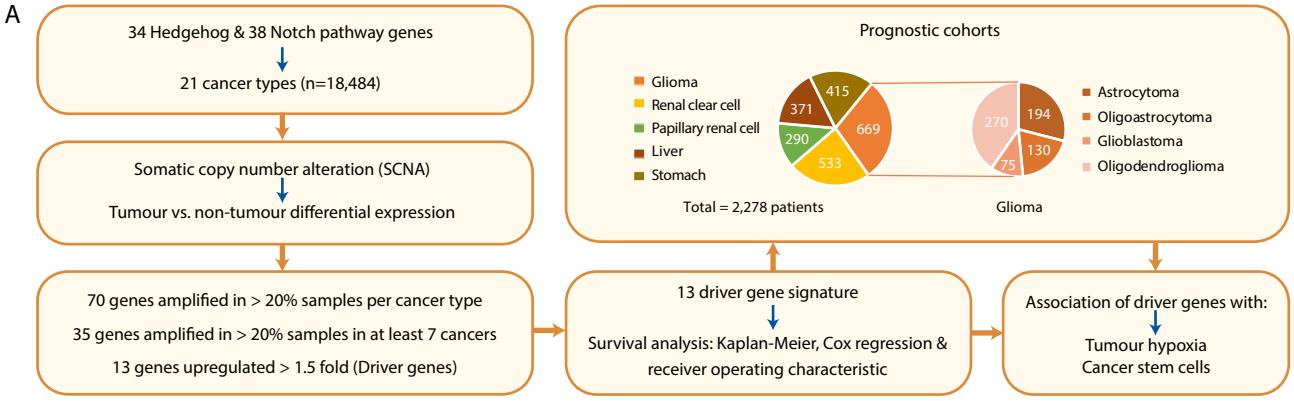
A
34 Hedgehog & 38 Notch pathway genes
21 cancer types (n=18,484)
Somatic copy number alteration (SCNA)
Tumour vs. non-tumour differential expression
70 genes amplified in > 20% samples per cancer type
35 genes amplified in > 20% samples in at least 7 cancers
13 genes upregulated > 1.5 fold (Driver genes)
Prognostic cohorts
Glioma
Renal clear cell
Papillary renal cell
Liver
Stomach
415
371
669
290
533
Total = 2,278 patients
270
194
130
75
Glioma
Astrocytoma
Oligoastrocytoma
Glioblastoma
Oligodendroglioma
13 driver gene signature
Survival analysis: Kaplan-Meier, Cox regression & receiver operating characteristic
Association of driver genes with:
Tumour hypoxia
Cancer stem cells

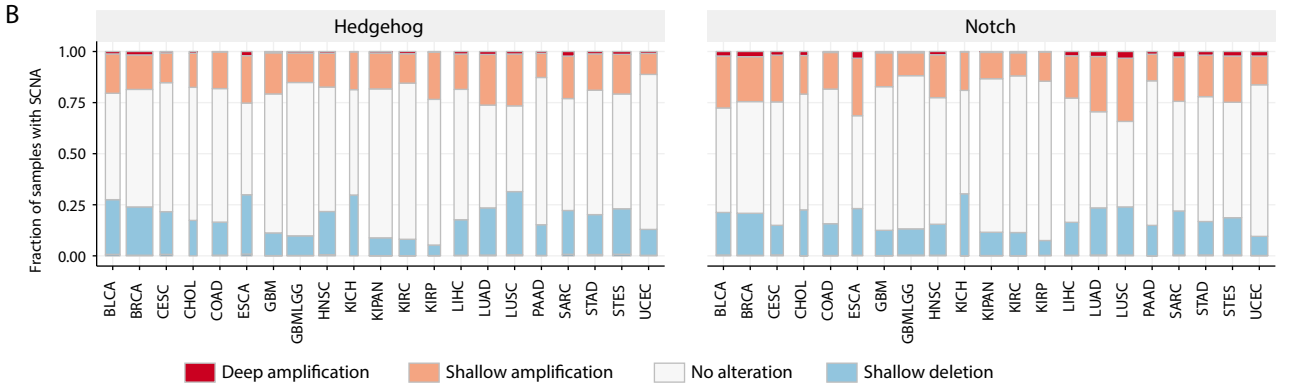
B
Hedgehog
Notch
Fraction of samples with SCNA
1.00
0.75
0.50
0.25
0.00
BLCA BRCA CESC CHOL COAD ESCA GBM GBMLGG HNSC KICH KIPAN KIRC KIRP LIHC LUAD LUSC PAAD SARC STAD STES UCEC
Deep amplification
Shallow amplification
No alteration
Shallow deletion

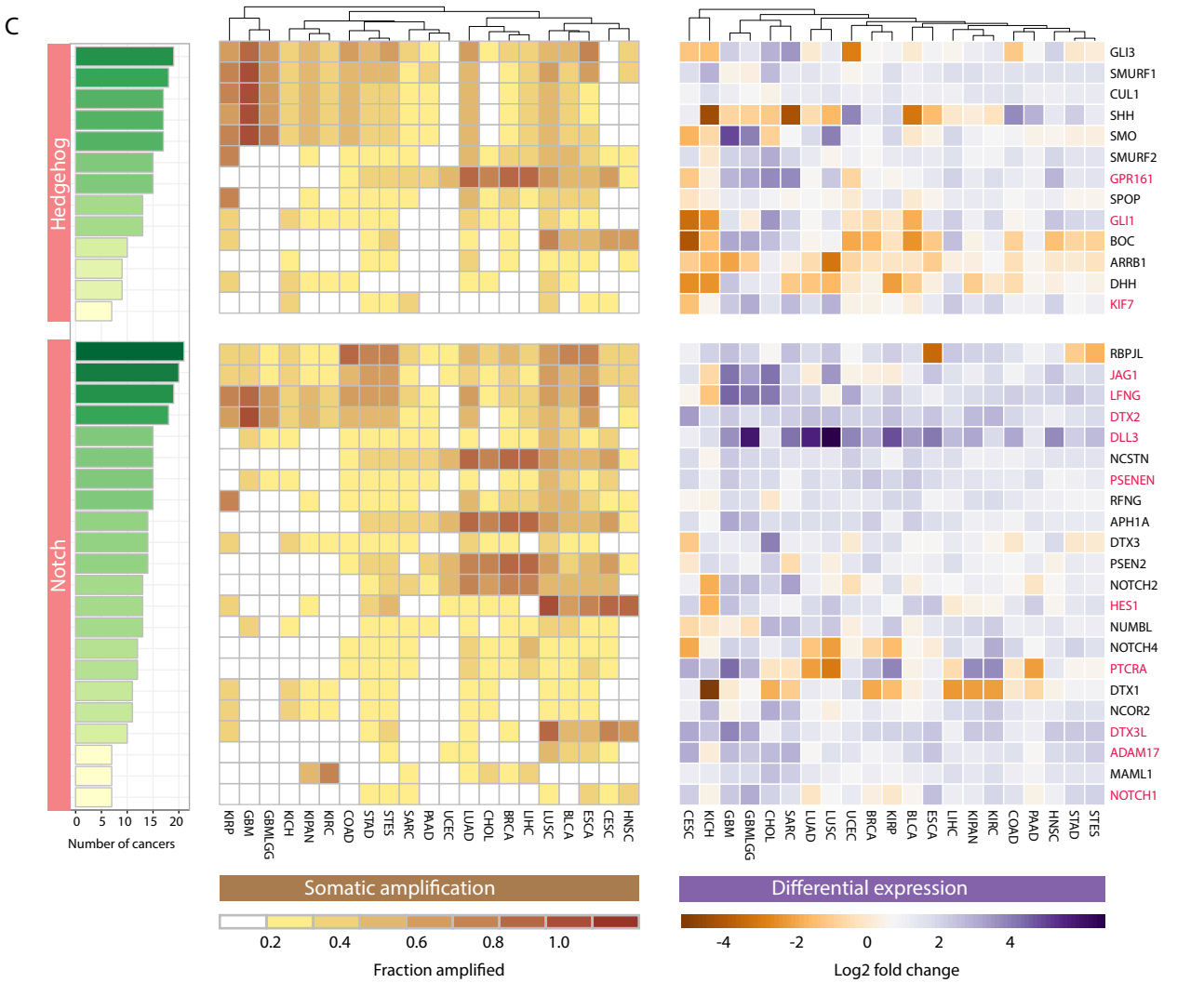
C
Hedgehog
Notch
0 5 10 15 20
Number of cancers
KIRP GBM GBMLGG KICH KIPAN KIRC COAD STAD STES SARC PAAD UCEC LUAD CHOL BRCA LIHC LUSC BLCA ESCA CESC HNSC
GLI3
SMURF1
CUL1
SHH
SMO
SMURF2
GPR161
SPOP
GLI1
BOC
ARRB1
DHH
KIF7
RBPJL
JAG1
LFNG
DTX2
DLL3
NCSTN
PSENEN
RFNG
APH1A
DTX3
PSEN2
NOTCH2
HES1
NUMBL
NOTCH4
PTCRA
DTX1
NCOR2
DTX3L
ADAM17
MAML1
NOTCH1
CESC KICH GBM GBMLGG CHOL SARC LUAD LUSC UCEC BRCA KIRP BLCA ESCA LIHC KIPAN KIRC COAD PAAD HNSC STAD STES
Somatic amplification
0.2 0.4 0.6 0.8 1.0
Fraction amplified
Differential expression
-4 -2 0 2 4
Log2 fold change

Figure 2

A

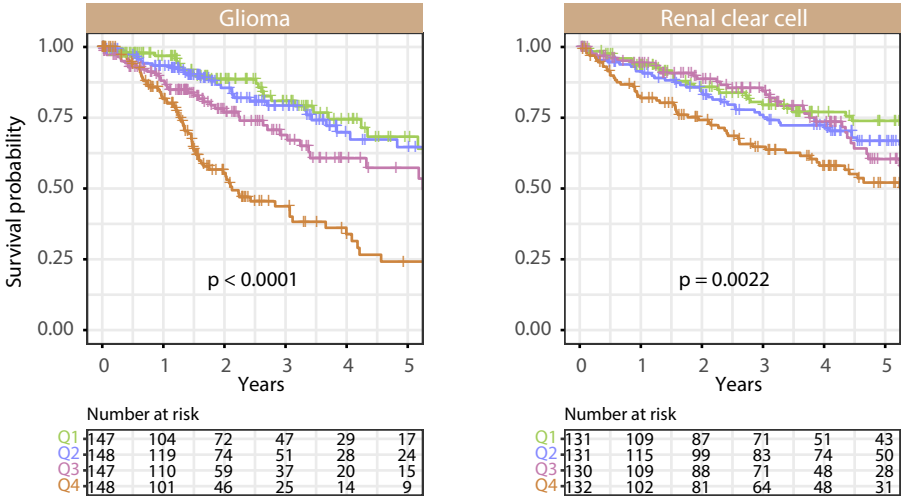
Glioma
Renal clear cell
Survival probability
1.00
0.75
0.50
0.25
0.00
p < 0.0001
p = 0.0022
0 1 2 3 4 5
Years
Number at risk
Q1 147 104 72 47 29 17
Q2 148 119 74 51 28 24
Q3 147 110 59 37 20 15
Q4 148 101 46 25 14 9
Q1 131 109 87 71 51 43
Q2 131 115 99 83 74 50
Q3 130 109 88 71 48 28
Q4 132 102 81 64 48 31

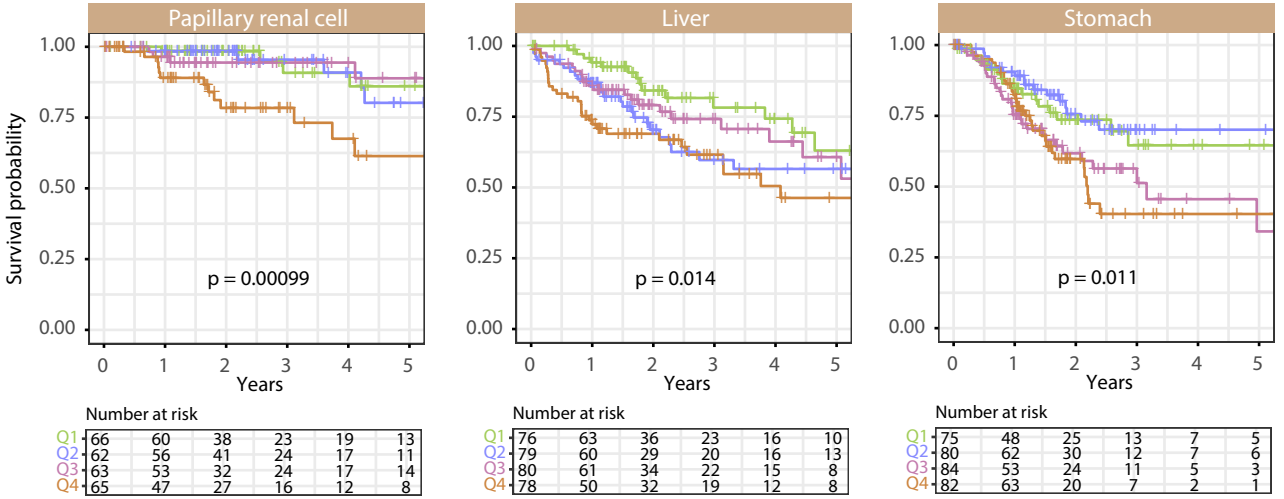
Papillary renal cell
Liver
Stomach
Survival probability
1.00
0.75
0.50
0.25
0.00
p = 0.00099
p = 0.014
p = 0.011
0 1 2 3 4 5
Years
Number at risk
Q1 66 60 38 23 19 13
Q2 62 56 41 24 17 11
Q3 63 53 32 24 17 14
Q4 65 47 27 16 12 8
Q1 76 63 36 23 16 10
Q2 79 60 29 20 16 13
Q3 80 61 34 22 15 8
Q4 78 50 32 19 12 8
Q1 75 48 25 13 7 5
Q2 80 62 30 12 7 6
Q3 84 53 24 11 5 3
Q4 82 63 20 7 2 1

B

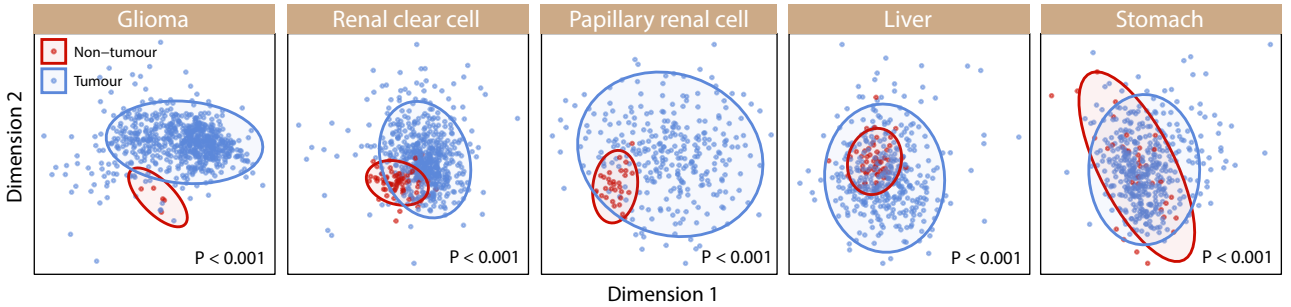
Glioma
Renal clear cell
Papillary renal cell
Liver
Stomach
Non−tumour
Tumour
Dimension 2
Dimension 1
P < 0.001
P < 0.001
P < 0.001
P < 0.001
P < 0.001

Figure 3

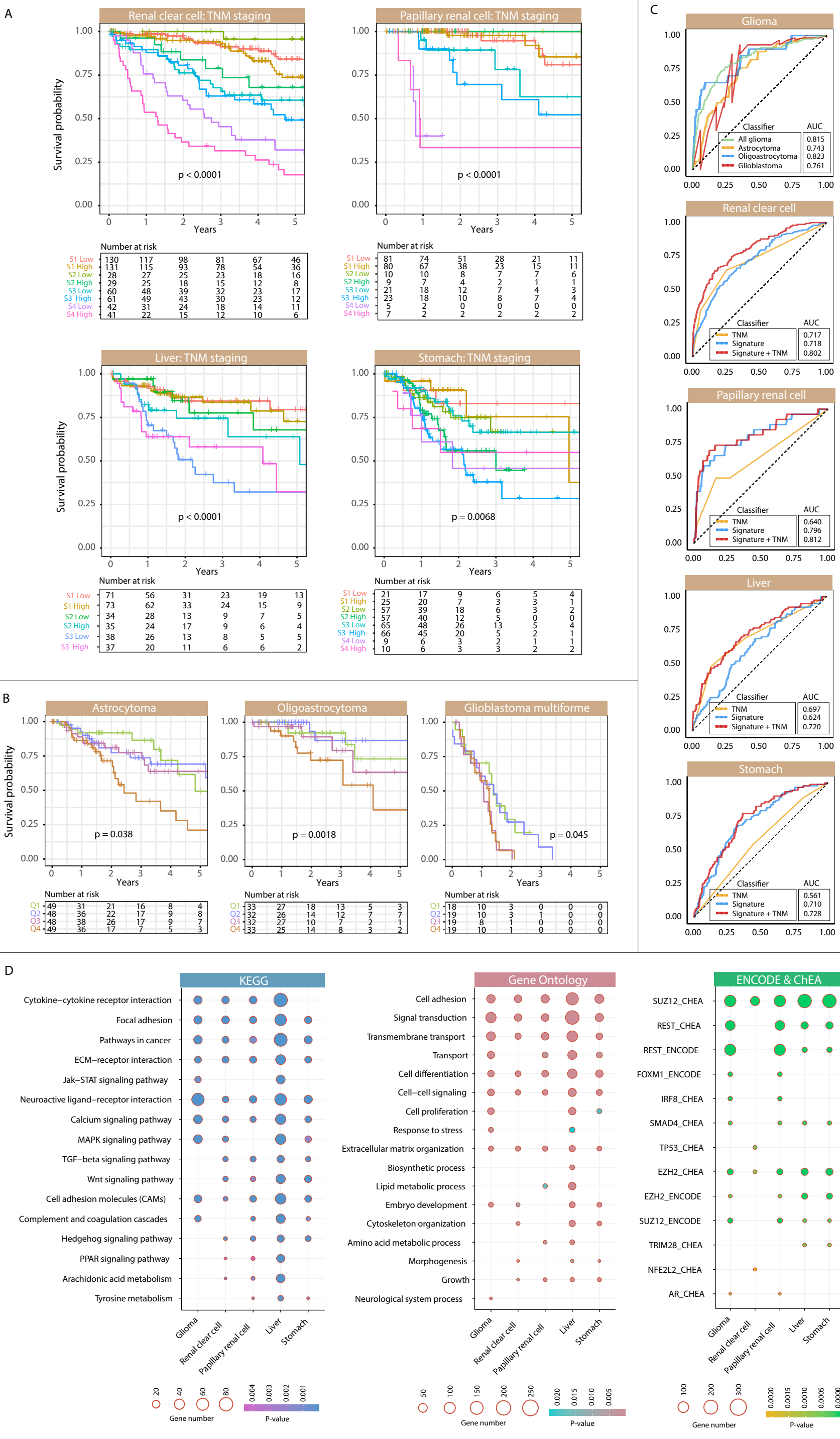
A
Renal clear cell: TNM staging
Papillary renal cell: TNM staging
Liver: TNM staging
Stomach: TNM staging
Survival probability
Years
p < 0.0001
p < 0.0001
p < 0.0001
p = 0.0068
Number at risk
S1 Low 130 117 98 81 67 46
S1 High 131 115 93 78 54 36
S2 Low 28 27 25 23 18 16
S2 High 29 25 18 15 12 8
S3 Low 60 48 39 32 23 17
S3 High 61 49 43 30 23 12
S4 Low 42 31 24 18 14 11
S4 High 41 22 15 12 10 6
S1 Low 81 74 51 28 21 11
S1 High 80 67 38 23 15 11
S2 Low 10 10 8 7 7 6
S2 High 9 7 4 2 1 1
S3 Low 21 18 12 7 4 3
S3 High 23 18 10 8 7 4
S4 Low 5 2 0 0 0 0
S4 High 7 2 2 2 2 2
S1 Low 71 56 31 23 19 13
S1 High 73 62 33 24 15 9
S2 Low 34 28 13 9 7 5
S2 High 35 24 17 9 6 4
S3 Low 38 26 13 8 5 5
S3 High 37 20 11 6 6 2
S1 Low 21 17 9 6 5 4
S1 High 25 20 7 3 3 1
S2 Low 57 39 18 6 3 2
S2 High 57 40 12 5 0 0
S3 Low 65 48 26 13 5 4
S3 High 66 45 20 5 2 1
S4 Low 9 6 3 2 1 1
S4 High 10 6 3 3 2 2
B
Astrocytoma
Oligoastrocytoma
Glioblastoma multiforme
p = 0.038
p = 0.0018
p = 0.045
Q1 49 31 21 16 8 4
Q2 48 36 22 17 9 8
Q3 48 38 26 17 9 7
Q4 49 36 17 7 5 3
Q1 33 27 18 13 5 3
Q2 32 26 14 12 7 7
Q3 32 27 10 7 2 1
Q4 33 25 14 8 3 2
Q1 18 10 3 0 0 0
Q2 19 10 3 1 0 0
Q3 19 8 1 0 0 0
Q4 19 10 1 0 0 0
C
Glioma
Classifier AUC
All glioma 0.815
Astrocytoma 0.743
Oligoastrocytoma 0.823
Glioblastoma 0.761
Renal clear cell
Classifier AUC
TNM 0.717
Signature 0.718
Signature + TNM 0.802
Papillary renal cell
Classifier AUC
TNM 0.640
Signature 0.796
Signature + TNM 0.812
Liver
Classifier AUC
TNM 0.697
Signature 0.624
Signature + TNM 0.720
Stomach
Classifier AUC
TNM 0.561
Signature 0.710
Signature + TNM 0.728
D
KEGG
Cytokine–cytokine receptor interaction
Focal adhesion
Pathways in cancer
ECM–receptor interaction
Jak–STAT signaling pathway
Neuroactive ligand–receptor interaction
Calcium signaling pathway
MAPK signaling pathway
TGF–beta signaling pathway
Wnt signaling pathway
Cell adhesion molecules (CAMs)
Complement and coagulation cascades
Hedgehog signaling pathway
PPAR signaling pathway
Arachidonic acid metabolism
Tyrosine metabolism
Gene Ontology
Cell adhesion
Signal transduction
Transmembrane transport
Transport
Cell differentiation
Cell–cell signaling
Cell proliferation
Response to stress
Extracellular matrix organization
Biosynthetic process
Lipid metabolic process
Embryo development
Cytoskeleton organization
Amino acid metabolic process
Morphogenesis
Growth
Neurological system process
ENCODE & ChEA
SUZ12_CHEA
REST_CHEA
REST_ENCODE
FOXM1_ENCODE
IRF8_CHEA
SMAD4_CHEA
TP53_CHEA
EZH2_CHEA
EZH2_ENCODE
SUZ12_ENCODE
TRIM28_CHEA
NFE2L2_CHEA
AR_CHEA
Glioma
Renal clear cell
Papillary renal cell
Liver
Stomach
Gene number
P-value

Figure 4

A

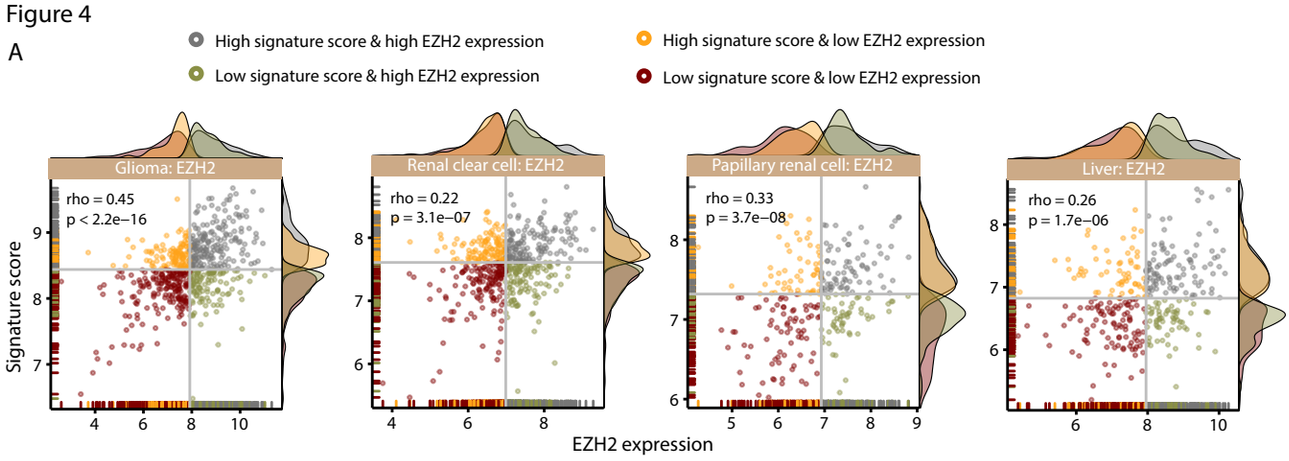

B

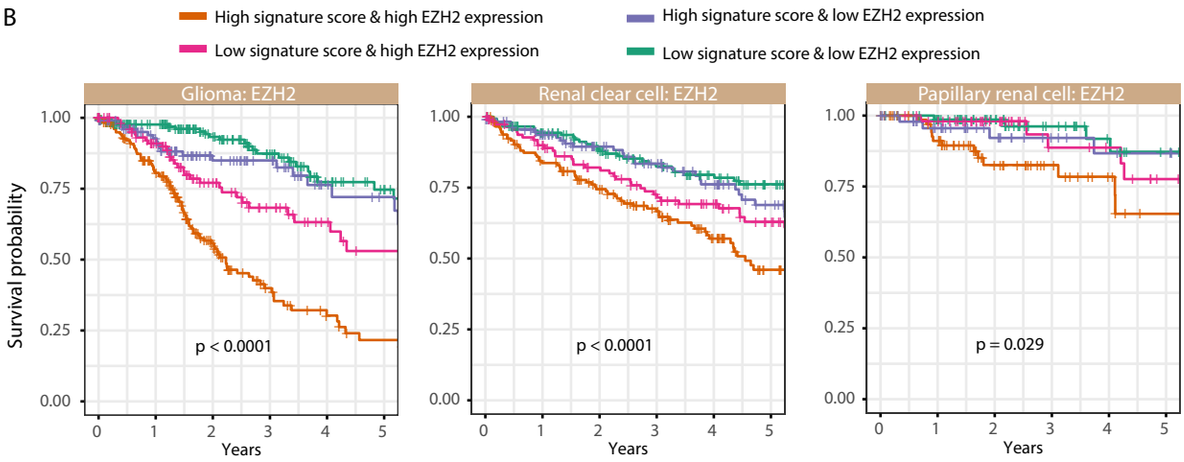

Number at risk

182	139	96	65	37	27
185	130	58	27	15	9
111	82	48	36	19	15
112	83	49	32	20	14

146	127	106	88	74	57
148	115	92	70	46	24
115	97	77	65	50	35
115	96	80	66	51	36

75	67	46	29	20	14
76	61	32	21	13	7
52	39	27	19	16	15
53	49	33	18	16	10

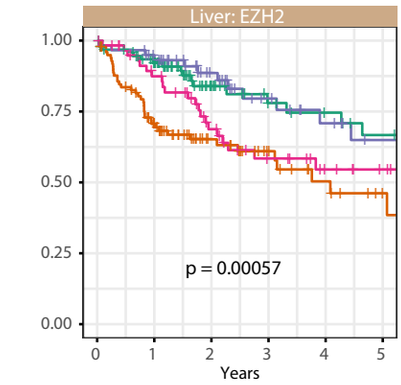

Number at risk

95	76	35	24	20	16
99	59	32	20	12	6
59	52	34	21	15	10
60	47	30	19	12	7

C

				Hazard Ratio (95% CI)	P -value
Glioma					
High signature score & high	EZH2	vs. low signature score & low	EZH2	5.141 (3.374 - 7.831)	2.48E-14
High signature score & low	EZH2	vs. low signature score & low	EZH2	1.475 (0.863 - 2.521)	0.15
Low signature score & high	EZH2	vs. low signature score & low	EZH2	1.936 (1.179 - 3.180)	0.0091
Renal clear cell					
High signature score & high	EZH2	vs. low signature score & low	EZH2	2.854 (1.884 - 4.353)	8.46E-07
High signature score & low	EZH2	vs. low signature score & low	EZH2	1.360 (0.835 - 2.215)	0.22
Low signature score & high	EZH2	vs. low signature score & low	EZH2	1.759 (1.116 - 2.774)	0.015
Papillary renal cell					
High signature score & high	EZH2	vs. low signature score & low	EZH2	4.391 (1.427 - 13.513)	9.90E-03
High signature score & low	EZH2	vs. low signature score & low	EZH2	1.856 (0.498 - 6.924)	0.35
Low signature score & high	EZH2	vs. low signature score & low	EZH2	2.008 (0.566 - 7.119)	0.28
Liver					
High signature score & high	EZH2	vs. low signature score & low	EZH2	2.685 (1.540 - 4.683)	5.00E-04
High signature score & low	EZH2	vs. low signature score & low	EZH2	1.089 (0.548 - 2.163)	0.81
Low signature score & high	EZH2	vs. low signature score & low	EZH2	1.886 (1.009 - 3.524)	0.046

D

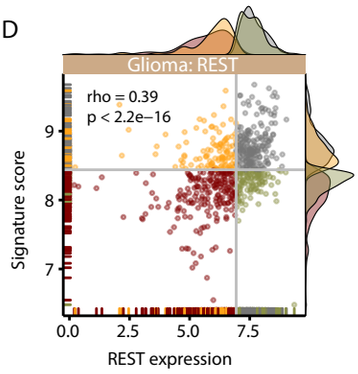

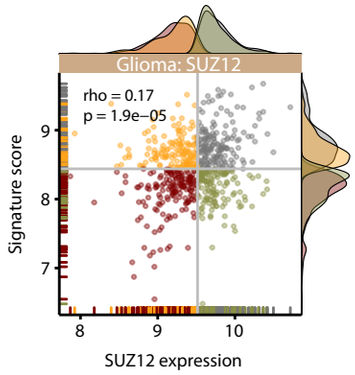

High signature score & high REST/SUZ12 expression
Low signature score & high REST/SUZ12 expression
High signature score & low REST/SUZ12 expression
Low signature score & low REST/SUZ12 expression

E

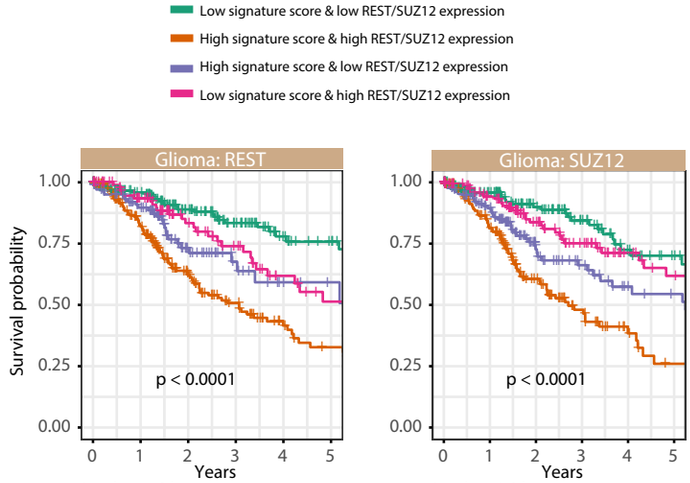

Number at risk

188	143	96	63	37	28
190	132	71	45	25	17
106	80	35	18	9	7
106	79	49	34	20	13

160	117	79	52	31	22
161	112	57	30	14	7
135	100	49	33	20	17
134	105	66	45	26	19

F

				Hazard Ratio (95% CI)	P -value
Glioma					
High signature score & high	REST	vs. low signature score & low	REST	3.646 (2.461 - 5.402)	1.12E-10
High signature score & low	REST	vs. low signature score & low	REST	1.811 (1.097 - 2.990)	0.02
Low signature score & high	REST	vs. low signature score & low	REST	1.626 (0.994 - 2.658)	0.053
Glioma					
High signature score & high	SUZ12	vs. low signature score & low	SUZ12	3.596 (2.332 - 5.545)	7.03E-09
High signature score & low	SUZ12	vs. low signature score & low	SUZ12	1.956 (1.227 - 3.118)	0.0048
Low signature score & high	SUZ12	vs. low signature score & low	SUZ12	1.210 (0.737 - 1.987)	0.45

Figure 5

A

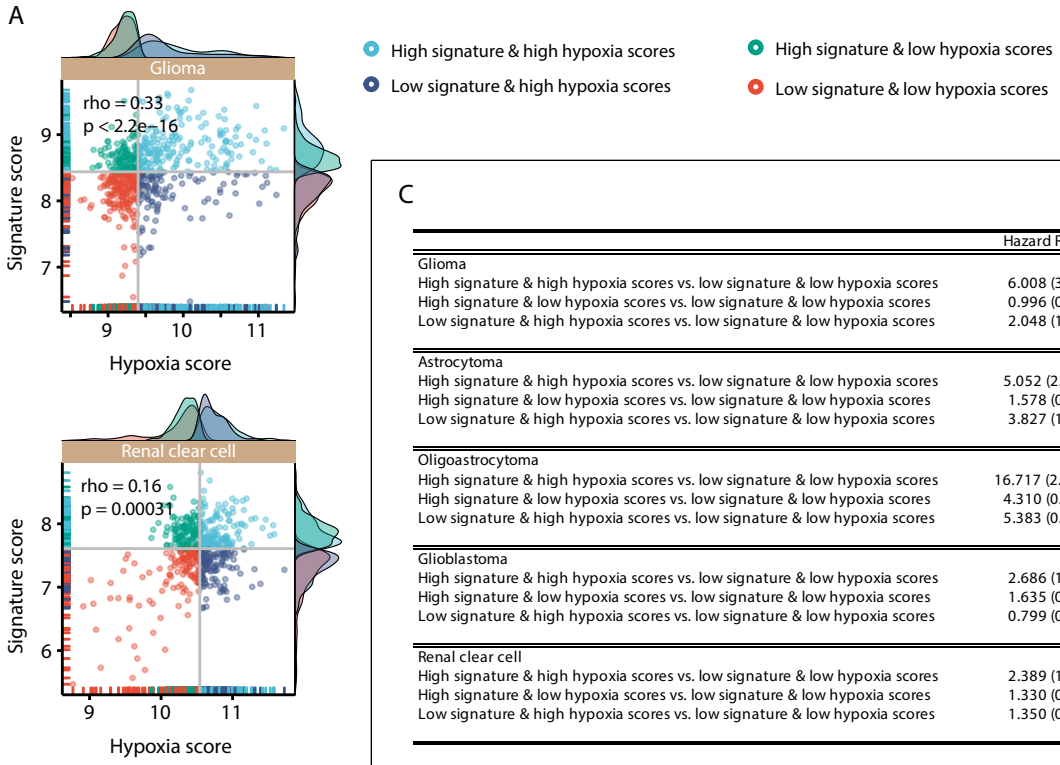

C

	Hazard Ratio (95% CI)	P -value
Glioma		
High signature & high hypoxia scores vs. low signature & low hypoxia scores	6.008 (3.939 - 9.161)	2.00E-16
High signature & low hypoxia scores vs. low signature & low hypoxia scores	0.996 (0.545 - 1.821)	0.98
Low signature & high hypoxia scores vs. low signature & low hypoxia scores	2.048 (1.245 - 3.367)	0.0047
Astrocytoma		
High signature & high hypoxia scores vs. low signature & low hypoxia scores	5.052 (2.292 - 11.134)	5.89E-05
High signature & low hypoxia scores vs. low signature & low hypoxia scores	1.578 (0.589 - 4.223)	0.36
Low signature & high hypoxia scores vs. low signature & low hypoxia scores	3.827 (1.571 - 9.322)	0.0031
Oligoastrocytoma		
High signature & high hypoxia scores vs. low signature & low hypoxia scores	16.717 (2.189 - 127.670)	6.60E-03
High signature & low hypoxia scores vs. low signature & low hypoxia scores	4.310 (0.447 - 41.540)	0.21
Low signature & high hypoxia scores vs. low signature & low hypoxia scores	5.383 (0.646 - 44.830)	0.12
Glioblastoma		
High signature & high hypoxia scores vs. low signature & low hypoxia scores	2.686 (1.151 - 6.270)	2.20E-02
High signature & low hypoxia scores vs. low signature & low hypoxia scores	1.635 (0.771 - 3.473)	0.2
Low signature & high hypoxia scores vs. low signature & low hypoxia scores	0.799 (0.363 - 1.759)	0.58
Renal clear cell		
High signature & high hypoxia scores vs. low signature & low hypoxia scores	2.389 (1.575 - 3.625)	4.23E-05
High signature & low hypoxia scores vs. low signature & low hypoxia scores	1.330 (0.829 - 2.135)	0.24
Low signature & high hypoxia scores vs. low signature & low hypoxia scores	1.350 (0.857 - 2.126)	0.19

B

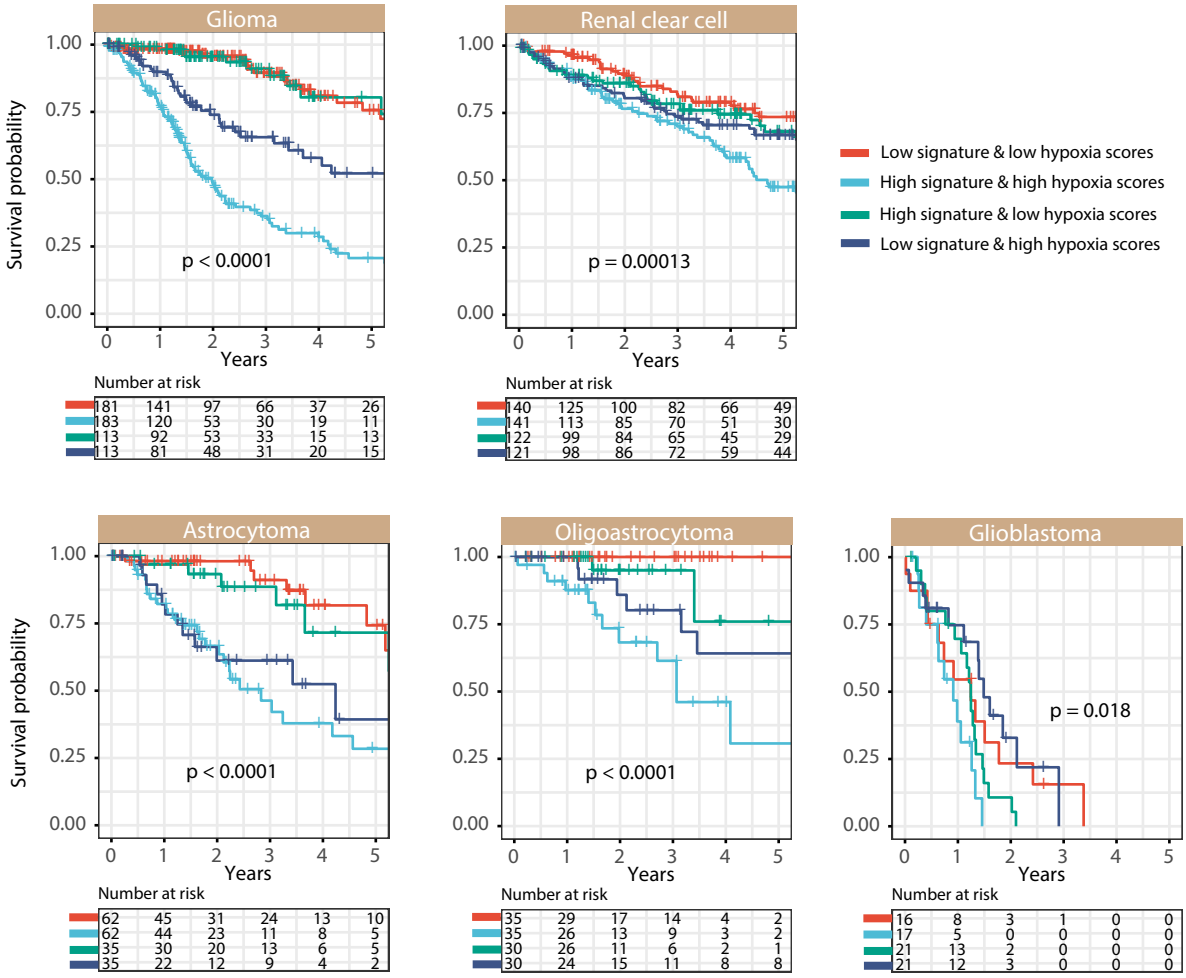

Figure 6

A

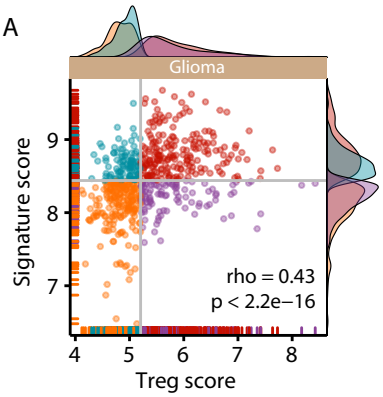

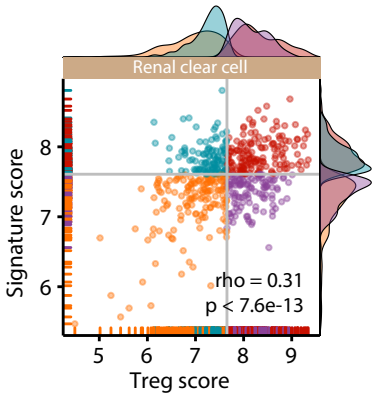

High signature & high Treg scores
Low signature & high Treg scores
High signature & low Treg scores
Low signature & low Treg scores

C

	Hazard Ratio (95% CI)	P -value
Glioma		
High signature & high Treg scores vs. low signature & low Treg scores	4.921 (3.277 - 7.391)	1.60E-14
High signature & low Treg scores vs. low signature & low Treg scores	1.671 (0.989 - 2.822)	0.055
Low signature & high Treg scores vs. low signature & low Treg scores	2.377 (1.459 - 3.872)	0.000503
Astrocytoma		
High signature & high Treg scores vs. low signature & low Treg scores	2.721 (1.398 - 5.298)	3.20E-03
High signature & low Treg scores vs. low signature & low Treg scores	1.288 (0.561 - 2.960)	0.55
Low signature & high Treg scores vs. low signature & low Treg scores	1.457 (0.597 - 3.554)	0.41
Oligoastrocytoma		
High signature & high Treg scores vs. low signature & low Treg scores	5.431 (1.522 - 19.374)	9.10E-03
High signature & low Treg scores vs. low signature & low Treg scores	2.470 (0.576 - 10.603)	0.22
Low signature & high Treg scores vs. low signature & low Treg scores	1.032 (0.222 - 4.804)	0.97
Glioblastoma		
High signature & high Treg scores vs. low signature & low Treg scores	3.065 (1.362 - 6.900)	0.0068
High signature & low Treg scores vs. low signature & low Treg scores	1.955 (0.824 - 4.639)	0.13
Low signature & high Treg scores vs. low signature & low Treg scores	1.274 (0.570 - 2.846)	0.55
Renal clear cell		
High signature & high Treg scores vs. low signature & low Treg scores	2.968 (1.922 - 4.582)	9.20E-07
High signature & low Treg scores vs. low signature & low Treg scores	1.649 (0.997 - 2.728)	0.051
Low signature & high Treg scores vs. low signature & low Treg scores	2.132 (1.342 - 3.385)	0.0013

B

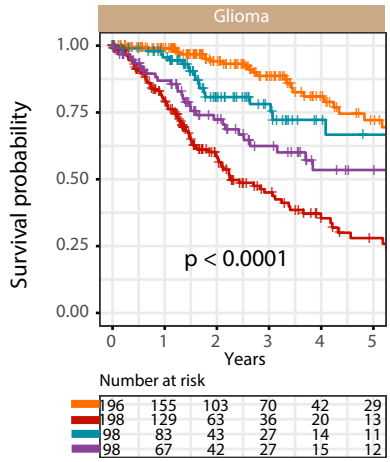

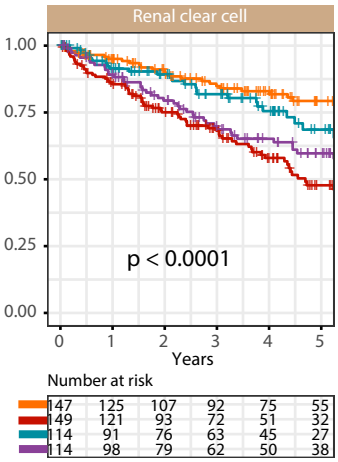

Low signature & low Treg scores
High signature & high Treg scores
High signature & low Treg scores
Low signature & high Treg scores